Title
Influences of North Pacific Ocean Domain Extent on the Western U.S. Winter Hydroclimatology in Variable-Resolution CESM

Journal
Journal of Geophysical Research: Atmospheres, 125(14)

ISSN
2169-897X

Authors
Rhoades, Alan M
Jones, Andrew D
O'Brien, Travis A
et al.

Publication Date
2020-07-27

DOI
10.1029/2019jd031977

Peer reviewed

Influences of North Pacific Ocean domain extent on the western US winter hydroclimatology in variable-resolution CESM

Alan M. Rhoades[1], Andrew D. Jones[1], Travis A. O'Brien[1], John P. O'Brien[2,1], Paul A. Ullrich[1,3], Colin M. Zarzycki[4]

[1]Lawrence Berkeley National Laboratory

[2]National Center for Atmospheric Research

[3]University of California, Davis

[4]Pennsylvania State University

Key Points:

- Three variable-resolution Community Earth System Model simulations are assessed for sensitivities to refinement domain size
- More extensive refinement of the Western Pacific reduces the integrated water vapor transport bias to the western US
- Topographic resolution and land-surface model have greater influences on simulated hydroclimatology than refinement domain extent

Corresponding author: Alan M. Rhoades, arhoades@lbl.gov

This article has been accepted for publication and undergone full peer review but has not been through the copyediting, typesetting, pagination and proofreading process which may lead to differences between this version and the Version of Record. Please cite this article as doi: 10.1029/2019JD031977

Abstract

Variable-resolution global climate models (VRGCMs) are a dynamical downscaling method that can reach spatiotemporal scales needed for regional climate assessments. Over the years, several users of VRGCMs have assumed where the location and extent of the refinement domain should be based on knowledge of the prevailing storm tracks and resolution dependence of important regional climate processes (e.g., atmospheric rivers [ARs] and orographic uplift), but the effect of high resolution domain size and extent on the simulation of downstream hydroclimatic phenomena has not been systematically evaluated. Here, we use variable-resolution in the Community Earth System Model (VR-CESM) to perform such a test. To do this, three VR-CESM grids were generated that span the entire, two-thirds, and one-third of the North Pacific and evaluated for a 30-year climatology using Atmospheric Model Intercomparison Project protocols. Simulations are compared with reanalysis products offshore (ERA5) and onshore (Livneh, 2015 and Parameter-elevation Regressions on Independent Slopes Model) of the western US. The westward expansion of refinement domain influenced integrated vapor transport (IVT), which was generally high-biased, but minimally impacted AR characteristics. Due to slight differences in landfalling AR counts in the western US, California winter precipitation generally improved with westward expansion of the refinement domain. Western US mountain snowpack and surface temperatures were insensitive to refinement domain size and were more influenced by changes in topographic resolution and/or land-surface model version. Given minimal dependence of simulated western US hydroclimate on refinement domain size over the North Pacific we advise future VR-CESM studies to focus grid resolution on better resolving land-surface heterogeneity.

1 Introduction

Given the cost prohibitive nature of executing uniform high-resolution global climate model (GCM) experiments (e.g., *Wehner et al.* [2014]; *Haarsma et al.* [2016]), dynamical downscaling has been fundamental in reaching the spatiotemporal scales necessary to meet regional climate information needs for assessments of vulnerability, impacts, and adaptation [*Giorgi*, 2019]. Over the last thirty years, regional climate models (RCMs) have been the primary means to perform dynamical downscaling, with various internationally coordinated projects aimed at producing climate impacts and/or model sensitivity analyses [*Christensen and Christensen*, 2007; *Giorgi et al.*, 2009; *der Linden and Mitchell*, 2009;

Mearns et al., 2012; *Evans et al.*, 2014]. These projects, and others, have shown that RCM simulations can provide added value over coarser-resolution GCM simulations through the enhanced representation of spatial variability in regions of complex terrain and land-sea contrast and more accurate simulations of certain weather features such as hurricanes [*Di Luca et al.*, 2015, 2016; *Poan et al.*, 2018].

Akin to RCMs, variable-resolution GCMs (VRGCMs) can be configured for high-resolution regional modeling, with computational cost scaling with the size and resolution of the most refined domain. Unique from RCMs, VRGCMs are GCMs that enable grid spacing to vary by location. This capability provides some advantages over RCMs, such as eliminating the need for two separate simulations and the corresponding biases that arise from the specification of lateral boundary conditions and coupling disparate models. However, VRGCMs also have their own issues, particularly scale sensitivity in sub-grid-scale parameterizations (e.g., shallow- and deep-convection, turbulence, and cloud macro-physics [*Arakawa and Jung*, 2011]). Over the last several decades, multiple VRGCMs have been developed and evaluated for various climate and weather applications. As discussed in *Fox-Rabinovitz et al.* [2006], VRGCMs were first developed as stretched-grid-GCMs that refine resolution in one location at the expense of coarsening another [*Yessad and Bénard*, 1996; *Côté et al.*, 1998; *Fox-Rabinovitz et al.*, 2001; *McGregor*, 2005]. More modern VRGCMs employ techniques that do not require grid-stretching, but rather gradual transitions in grid-refinement including the variable-resolution capabilities in the Community Earth System Model (VR-CESM; [*Zarzycki et al.*, 2014a; *Guba et al.*, 2014]), the Model for Prediction Across Scales (MPAS; [*Park et al.*, 2014; *Rauscher and Ringler*, 2014]), and the Finite Volume Cubed-Sphere Dynamical Core (FV3; [*Harris and Lin*, 2013; *Harris et al.*, 2016]). A more detailed summary of the current community of VRGCMs, and the specifics of their atmospheric model structural and parameter decisions, can be found in *Ullrich et al.* [2017].

The downscaling benefits and computational cost savings enabled by VRGCMs have been extensively evaluated across a hierarchy of model test-cases. *Rauscher et al.* [2013] and *Rauscher and Ringler* [2014] utilized idealized model test cases in MPAS, atmospheric dynamics enabled with prescribed physics (Held-Suarez) and atmospheric dynamics and physics enabled with "controlled" SSTs (aquaplanet), to show that VR refinement could positively impact eddy kinetic energy (i.e., storm tracks) in the mid-latitudes, but may have detrimental effects on model moist-physics in equatorial regions. Similarly, *Zarzy-*

cki et al. [2014b] used VR-CESM in an aquaplanet test-case and showed that the statistics derived from the VR refinement domain matched those of a corresponding uniform high-resolution simulation and noted that cross-scale interactions in the grid-transition region were physically consistent (e.g., Kelvin wave phase-speeds). In relation to the findings highlighted in *Rauscher et al.* [2013], the choice of and resolution dependence of the physics scheme was noted to be responsible for the detrimental feedbacks on cloud fraction, precipitation rates, and diabatic heating rates. Building on the aforementioned, *Sakaguchi et al.* [2015] used MPAS in a real-world-like model test case, atmosphere-land model coupling and prescribed SSTs and sea-ice observations (Atmospheric Model Intercomparison Project; AMIP), to show that when provided strong surface forcing (e.g., topography, SSTs, etc.) VR refined simulations provide comparably realistic process representation compared with uniform high resolution simulations (e.g., South American monsoon and Andean induced moisture convergence over the Amazon). More recently, *Sakaguchi et al.* [2016] used MPAS with AMIP protocols to explore how VR refinement may influence the large-scale circulation, both locally and globally, through "upscale effects" and found comparable improvements as those found in uniform high-resolution simulations (e.g., representation of synoptic wave activity and propagation and westerly jets) and alluded that this could improve simulated hydrologic extremes through changes in the advection of scalars (e.g., water vapor). This last point in *Sakaguchi et al.* [2016] is important and has not been extensively evaluated in the VRGCM literature to date, particularly the sensitivities of the simulated mean climate and hydrologic extremes due to the placement and/or extent of the refinement domain in VRGCMs in real-world-like model test cases.

In the RCM literature, the implications of domain extent, placement and resolution on the added value of downscaled simulations has been extensively explored [*Laprise et al.*, 2008; *Caron et al.*, 2011; *Caron and Jones*, 2012; *Diaconescu and Laprise*, 2013; *Di Luca et al.*, 2015; *Brisson et al.*, 2016; *Di Luca et al.*, 2016; *Matte et al.*, 2016; *Lucas-Picher et al.*, 2017; *Matte et al.*, 2017; *Poan et al.*, 2018]. In particular, careful selection of the RCM domain size and extent has been shown to have significant impacts on simulation fidelity [*Xue et al.*, 2014; *Matte et al.*, 2016, 2017]. The prevailing rule-of-thumb, colloquially termed the "Goldilocks" rule, is that the RCM domain size should not be too big, nor too small to allow for appropriate scale interactions between the lateral boundary conditions and the innermost model domain [*Jones et al.*, 1995]. As shown in *Leduc and Laprise* [2009], if the RCM domain is too small, there is insufficient time for meteorological processes to develop small-scale features (or transient eddies), particularly higher up in the troposphere where surface forcing is weak and winds are stronger. Yet if the RCM domain is too large, the features within the simulated domain can become decoupled from the large-scale forcing data [*Leduc and Laprise*, 2009; *Matte et al.*, 2016], particularly if domain nudging methods are not used [*Miguez-Macho et al.*, 2004]. Therefore, the RCM domain size should be "just right" with an even balance between the forces associated with the large-scale boundary conditions and transient eddy spin-up in the RCM domain(s) in order for the RCM to recreate and spatially enhance the GCM simulation. In a practical sense, this tradeoff also has significant implications with respect to computational expense of the simulation, with larger domains resulting in greater costs.

The "Goldilocks" rule evidenced in the RCM literature may also apply to VRGCMs, but to date has been sparsely studied. The VRGCM literature has primarily explored the role of horizontal resolution and sub-grid-scale parameterization sensitivities. In particular, *Hagos et al.* [2015] used both aquaplanet and real-world-like AMIP simulations in MPAS at ~240km to ~30km to explore resolution sensitivity of storm tracks and counts, in particular atmospheric rivers (ARs), over the North Pacific using uniform-resolution grids. For the AMIP simulations, the number of AR events that impinge on the western US showed little dependence on resolution at ~120 km vs ~30 km and were low compared with reanalysis estimates due to an overall drier subtropics and poleward-shifted storm track. Most recently, *Goldenson et al.* [2018] utilized MPAS-AMIP simulations with VR refinement over the western US coast at ~30 km and showed that the simulation of ARs was high biased compared with reanalysis, but improved compared with coarser uniform-resolution simulations and previous versions of MPAS with differing dynamical cores and sub-grid-scale physics parameterizations. Similar to MPAS-based studies, a plethora of VR-CESM-based studies has been published that assess the resolution and sub-grid-scale physics dependence of simulations across the continental US. For example, VR-CESM has shown comparable skill in reproducing results from a uniform high-resolution GCM simulation across a hierarchy of simulations including baroclinic wave tests, aquaplanet, and full physics test-cases over the continental US [*Gettelman et al.*, 2018], extratropical and tropical cyclone characteristics [*Zarzycki and Jablonowski*, 2014; *Zarzycki et al.*, 2015, 2016; *Zarzycki*, 2016] and has been shown to produce comparable results to RCMs in coastal and mountain climates [*Huang et al.*, 2016; *Huang and Ullrich*, 2016, 2017; *Rhoades et al.*, 2016, 2018a,b; *Wang and Ullrich*, 2018; *Wang et al.*, 2018; *Wu et al.*, 2017, 2018; *Xu et al.*, 2018; *Burakowski et al.*, 2019; *Rahimi et al.*, 2019; *van Kampenhout et al.*, 2019]. Yet, akin to the aforementioned MPAS studies, most have assumed what size the refinement domain should be for their particular regional application by identifying the region's prevailing storm direction, resolution dependence of the most extreme storms, and necessary resolution to appropriately characterize the surface heterogeneity. Given the aforementioned literature on the "Goldilocks" rule in shaping the climate information produced by RCMs, the effect of refinement domain size and placement on the simulated storm characteristics that shape regional hydroclimates needs to be explored in VR-CESM as well.

Evaluation of regional hydroclimate, particularly in mountainous regions, has shown a clear added value of dynamical downscaling approaches [*Xue et al.*, 2014]. Accurately capturing regional hydroclimate requires models to represent multiple spatiotemporal scales and large-scale teleconnections, the near surface and free atmosphere, and statistical moments – as pointed out by *Di Luca et al.* [2015] this is essential in evaluating the added value of a particular downscaling approach. Furthermore, hydroclimatic extremes can have significant socioeconomic impacts, particularly on water management [*Ullrich et al.*, 2018; *Vano et al.*, 2019], and should be a model benchmark if the end-goal of model development is usability outside of academic circles. The western US provides a useful multi-scale domain test bed as the hydroclimatology is largely shaped by inter-annual variability caused by large-scale teleconnections (e.g., El Niño Southern Oscillation, ENSO; [*Harrison and Larkin*, 1998; *Williams and Patricola*, 2018; *O'Brien et al.*, 2019; *Patricola et al.*, 2019]) and hydrometeorological extremes (e.g., ARs; [*Ralph et al.*, 2018, 2019]). In particular, ARs have been shown to be crucial to western US accumulated precipitation totals. Notably, California receives 50% of its water year totals in under 10-40 (60-120) hours in the southern (northern) part of the State [*Lamjiri et al.*, 2018] with an average of 14 landfalling ARs per year [*Neiman et al.*, 2008]. ARs also directly influence inter-annual variability in mountain snowpack with estimates ranging between 22-73% of annual snowpack totals associated with ARs in the California Sierra Nevada [*Guan et al.*, 2013]. Greater flood potential in California is also associated with ARs due to their punctuated extreme precipitation totals when combined with saturated soil moisture conditions [*Ralph et al.*, 2006] and/or large antecedent snowpacks [*Guan et al.*, 2016; *White et al.*, 2019]. Over the years, several GCM simulations at 1° and 0.5° resolution have shown skill in representing AR characteristics over the North Pacific [*Dettinger*, 2011], CESM being one

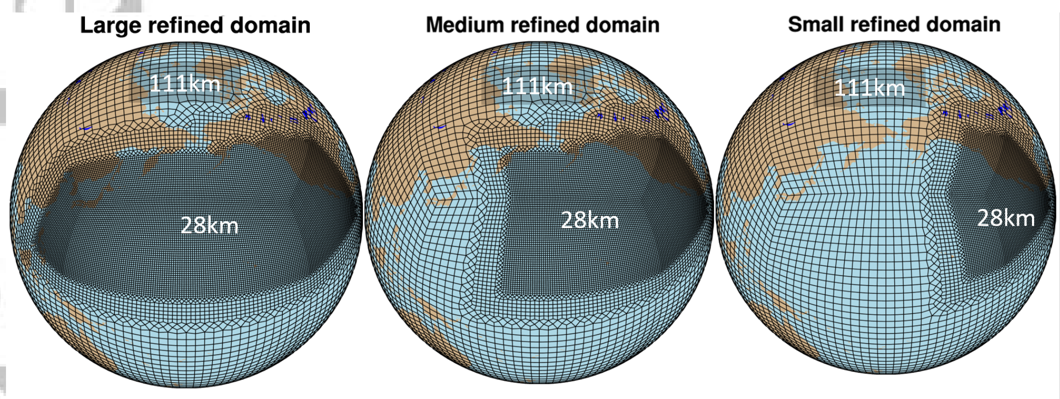

Figure 1. The three VR-CESM grids used for this study. Each cubed-sphere grid has a quasi-uniform 111km (1.00°) global resolution and a 28km (0.25°) refinement region over the north Pacific and western US.

such model [*Hagos et al.*, 2016; *Shields and Kiehl*, 2016a,b; *Benedict et al.*, 2019]. It was noted in some of these studies that commonly used GCM resolutions may bias the interactions between landfalling ARs and orography. With that said, VR-CESM provides a model framework to explore the interactions between refinement domain size and fidelity in representing AR characteristics over the North Pacific and the interactions between landfalling ARs and their influence on the simulated western US hydroclimate.

To evaluate the "Goldilocks" rule in VR-CESM, we have designed an experiment where a 28km refinement domain size varies longitudinally, yet is fixed latitudinally, over the North Pacific Ocean basin. Our hypothesis is that these different model configurations will modify the simulated hydroclimatology of the western US through its impact on the dynamic and thermodynamic processes that influence key storm types (e.g., ARs). The remainder of the paper is organized as follows: Section 2 discusses the experimental design for the VR-CESM domain sensitivity experiments and the reanalysis datasets, statistical approaches, and atmospheric river detector used to benchmark model performance. Section 3 includes the results of the study, followed by the discussion and conclusions outlined in section 4.

2 Experimental Design and Reference Datasets

CESM Overview

CESM is a widely used and community-supported GCM co-developed by the National Center for Atmospheric Research (NCAR) and the US Department of Energy (DoE) over the last several decades and is comprised of stand-alone atmospheric, land-surface, oceanic, sea-ice, and land-ice components that can either be fully and/or selectively coupled or data prescribed [*Collins et al.*, 2006; *Gent et al.*, 2011; *Hurrell et al.*, 2013]. For the domain size sensitivity simulations, we chose to use the Atmosphere Model Intercomparison Project (AMIP) protocols with active, coupled atmosphere and land-surface, and prescribed ocean and sea-ice models using monthly observations of sea-surface temperature and sea-ice extent [*Gates et al.*, 1999; *Hurrell et al.*, 2008]. Figure 1 depicts the three VR-CESM grids that were generated using an open-source grid generator, SQuadGEN [*Guba et al.*, 2014; *Ullrich*, 2014]. The three VR-CESM grids span resolutions of 111km->55km->28km (not including grid-transition regions) with a fixed latitudinal extent (i.e., 15°N to 60°N), a fixed eastern boundary (100°W), and a varied longitudinal extent of 141 degrees (large refined domain), 94 degrees (medium refined domain), and 47 degrees (small refined domain) over the North Pacific Ocean. The latitudinal and longitudinal extents of the 28km refinement domain were chosen based on work done by *Payne and Magnusdottir* [2014], who identified AR source-to-terminus pathways using the Modern-Era Retrospective Analysis for Research and Applications (MERRA) reanalysis data. Each of the VR-CESM simulations were run from 1984-2015, with 1984 discarded as spin-up. Table 1 provides a summary of the aforementioned and highlights the number of grid elements, simulated years per day using 48 nodes on the National Energy Research Scientific Computing Center (NERSC) Cori-Haswell supercomputer, and the simulation output frequencies.

The atmospheric model used for these experiments was the Community Atmosphere Model (CAM) version 5.4 with the cubed-sphere spectral element (CAM5.4-SE) dynamical core, which features variable-resolution capabilities and demonstrated computational scalability [*Dennis et al.*, 2012]. The CAM5.4-SE physics time-step for each simulation was set to 7.5 minutes (4 times shorter than the default), and the convective time-scale parameter (tau) is set to 15 minutes (2 times shorter than the default). These timescales were chosen to more comprehensively capture processes governing the finer features simulated in the high-resolution domain. In addition, we utilized the newest publicly released version of the Morrison and Gettelman microphysics scheme, version 2 (MG2), which allows for prognostic rainfall and snowfall [*Gettelman and Morrison*, 2015; *Gettelman et al.*, 2015], an essential feature to simulate mountainous hydroclimate correctly [*Rhoades et al.*, 2018b]. All other physics parameterizations and prescription files are default to the CAM5 release including bulk aerosols [*Ghan et al.*, 2012], deep convection [*Neale et al.*, 2008], macrophysics [*Park et al.*, 2014], radiation [*Iacono et al.*, 2008], and shallow convection [*Park and Bretherton*, 2009]. Further specifics of CAM-SE can be found in *Neale et al.* [2010] and *Lauritzen et al.* [2018].

The newest version of the Community Land Model available at time of writing, version 5 with satellite phenology (CLM5.0-SP), was used. CLM5.0-SP was chosen as it has considerable process advancements compared with CLM4.0-SP and CLM4.5-SP such as carbon and nitrogen cycling, soil evaporation and decomposition, vegetation hydraulics and traits, representative hillslope based river routing, surface and subsurface hydrology and, in particular to western US hydroclimate, snow hydrology [*Lawrence et al.*, 2019]. The snow hydrology module in CLM5.0-SP explicitly models the mass of water, the mass of ice, layer thickness, and temperature. Compared with CLM4.0-SP, CLM5.0-SP includes 12 dynamic snow layers (rather than 5), enables snow water equivalent to develop to 10-meters (rather than 1-meter), calculates the snow cover fraction separately for the accumulation and melt phases of the snow season, and allows the forest canopy to capture and store ice and liquid precipitation separately (rather than just liquid precipitation). Further, snow cover depletion in CLM5.0-SP now depends on the ratio of the current and maximum mass of snow and a melt parameter that accounts for sub-grid-scale topographic variability. Furthermore, the bulk density of snow now depends on both temperature and wind (rather than just temperature) [*van Kampenhout et al.*, 2017]. Similar to CLM4.0-SP, CLM5.0-SP allows for black carbon, organic carbon, and dust deposited and encapsulated by the snowpack. The snowpack layers are then free to compact and age by pressure and melt.

Reference Dataset Overview

We evaluate our VR-CESM simulations against three reanalysis products: ERA5 [*Copernicus Climate Change Service (C3S)*, 2017], Livneh, 2015 (L15; [*Livneh et al.*, 2015]) and the Parameter-elevation Relationships on Independent Slopes Model (PRISM; [*Daly et al.*, 2008]). All reference datasets in this study were either conservatively (L15 and PRISM, original data ≤28km resolution) or bilinearly (ERA5, original data ≥28km resolution) interpolated using TempestRemap [*Ullrich and Taylor*, 2015; *Ullrich et al.*, 2016] from their base resolutions to the highest resolution of the VR-CESM simulations (i.e., 28km). Similarly, each of the VR-CESM simulations are bilinearly interpolated from

Table 1. VR-CESM North Pacific Ocean domain size experiment metadata including the case name, number of spectral elements in the model grid, simulated years per day (SYPD), and 28km domain size extent in latitude and longitude. All CESM simulations were conducted for 1984-2015 with all of 1984 discarded as spin-up. For each of the CESM simulations all default CAM5.4-SE variables were output at monthly intervals, most variables (including those from CLM5.0-SP) were output at daily intervals, and a select number of CAM5.4-SE variables were output at 6-hourly, 3-hourly, and 1-hourly intervals to evaluate atmospheric rivers.

CESM Case Name	*Number of Spectral Elements*	*SYPD* (48 *nodes*)	28*km Refinement Domain Extent*
Large refined domain	17,715	3.74	Lat: 15N to 60N Lon: 119E to 100W
Medium refined domain	13,905	4.25	Lat: 15N to 60N Lon: 166E to 100W
Small refined domain	9,879	4.55	Lat: 15N to 60N Lon: 147W to 100W
No refined domain	5,400	8.47	N/A

unstructured to regular latitude–longitude at 28km resolution over the entire extent of the largest refined domain. ERA5 was used to evaluate offshore fields in VR-CESM, whereas PRISM and L15 were used for onshore fields. When comparing the climatological and seasonal differences between model simulations and reanalysis products, we utilize the Kolmogorov-Smirnov two-sample test made available from the NCAR Command Language [*The NCAR Command Language (Version 6.6.2)*, 2019]. To ensure that we minimize Type-I error in spatial map comparisons we also employ the false discovery rate (FDR; *Benjamini and Hochberg* [1995]; *Wilks* [2016]) combined with a strict p-value choice (i.e., 0.001).

ERA5 is a newly available fifth generation reanalysis product developed at the European Centre for Medium-Range Weather Forecasts (ECMWF) that uses a mixture of aircraft, satellite, and in-situ measurement data assimilated into the Integrated Forecasting System (IFS) to estimate climate variables globally across 137 vertical levels at 30km spatial and hourly temporal resolution. To evaluate domain size influence on integrated vapor transport (IVT), and therefore AR activity, ERA5 zonal and meridional winds and specific humidity across 17 vertical levels, or every 50 hPa, were used. The 17 vertical levels include: 100, 150, 200, 250, 300, 350, 400, 450, 500, 550, 600, 650, 700, 750, 800, 850, 900, 950, and 1000 hPa. In comparison, CAM5.4-SE has 32 terrain-following vertical levels which include: 4, 8, 14, 25, 36, 43, 52, 62, 74, 88, 103, 122, 143, 168, 198, 233, 274, 322, 379, 446, 525, 610, 691, 763, 821, 860, 887, 913, 936, 957, 976, and 993 hPa (as well as the terrain surface). To evaluate potential IVT sensitivity to vertical level choice in ERA5 an analysis, not shown, was conducted across a smaller time-period (2006-2015) to evaluate how the number of vertical levels used in ERA5 (17 vs 38) would impact computed IVT. An average difference over the North Pacific of ~20 kg/m/s was found (or a ~10% difference).

L15 utilizes 21,137 quality assured and quality controlled in-situ meteorological stations that encompass a large swath of spatial coverage of North America and a temporal period of 1950-2013. *Livneh et al.* [2015] then applies several adjustments to the in-situ derived meteorological variables using NCEP-NCAR reanalysis data along with other key spatiotemporal adjustments such as correcting the climate normal fields towards PRISM, assuming a fixed lapse-rate of 6.5 K/km, and modifications to orographic precipitation. This spatially continuous daily meteorological field is then used to bound variable infiltration capacity (VIC) hydrologic model simulations that then output key hydroclimate variables (e.g., snow water equivalent) to produce a 6km resolution reanalysis product.

PRISM was developed at Oregon State University and is a spatially continuous high-resolution estimate (either 800m, proprietary, or 4km, free) of precipitation, max and min surface temperature, max and min surface vapor pressure deficit, and mean dewpoint temperature over the continental US for the time period of 1970 to present day. To create the spatially continuous climate fields, *Daly et al.* [2008] used a digital elevation model and quality assurance and quality control protocols on ~13,000 precipitation and ~10,000 temperature in-situ measurement stations. To ensure that proper spatiotemporal variation was incorporated into the PRISM climate fields, their algorithm incorporated geographic variables, including coastal proximity, elevation, location, terrain slope, topographic orientation and position, and vertical atmospheric layer. PRISM was used for this analysis due to its improved characterization of coastal effects, cold air drainage, elevational gradients, inversion layers, and rain shadows compared with other publicly available reanalysis products.

The use of both PRISM and L15 provides juxtaposition for known tradeoffs in reanalysis products widely used in the western US hydroclimate community. For example, the assumption of a fixed lapse rate of 6.5 K/km in L15 has been shown to be particularly influential on minimum surface temperature in mountainous regions [*Walton and Hall*, 2018]. Similarly, L15 and PRISM (and other reanalysis products) have shown considerable differences in precipitation amount and structure due to differences in spatial interpolation technique and quality controls used to account for the spatiotemporal variation of measurement networks and extreme events, particularly at higher elevation in mountainous regions [*Henn et al.*, 2018a,b; *Timmermans et al.*, 2019]. Further, as discussed in *Rhoades et al.* [2018c], L15 is one of only a handful of reanalysis products that provide daily snow water equivalent estimates across the western US and has shown comparable skill to a high quality snow water equivalent reanalysis product that is only available in the California Sierra Nevada, the Sierra Nevada Snow Reanalysis (SNSR; [*Margulis et al.*, 2016]).

Atmospheric River Tracking with TempestExtremes

To evaluate the potential influence of domain size on AR characteristics, we employ a publicly-available Lagrangian tracking algorithm, TempestExtremes [*Ullrich and Zarzycki*, 2017; *Zarzycki and Ullrich*, 2017]. Specifically, the AR algorithm in TempestExtremes when used "out-of-the-box" has tended to be a good representation of the median of the community of AR trackers [*Shields et al.*, 2018]. For detecting ARs, TempestExtremes necessitates the use of five parameter choices to filter fields of IVT. The parameter definitions (units) and our choices include:

(1) minimum threshold of IVT to be considered an AR (min_val; kg m^{-1} s^{-1}) = 250
(2) minimum laplacian of IVT (min_laplacian; kg m^{-1} s^{-1} $degrees^{-2}$) = 50000 (default)
(3) minimum area of IVT to be classified as an AR (min_area; # of grid-cells) = 25
(4) radius of the discrete Laplacian (size_laplacian; # of grid-cells) = 35
(5) absolute latitude at which AR detection is not warranted (min_abslat; degrees) = 15

These choices are specific to the 28km grid on which major analysis for this study is performed. To choose the AR algorithm parameters we use a combination of AR community suggested values (e.g., min_val and min_area, *Ralph et al.* [2018]) and conducted a parameter sensitivity analysis (e.g., min_laplacian, size_laplacian, and min_abslat). The AR algorithm generated fields are then stitched together in time using another TempestExtremes algorithm that we set to have an overlap constraint of, at least, 8 time steps (or 2 days with 6-hourly data) and, at least, 35 grid-cells (which meets the *Ralph et al.* [2018] average AR width constraint of 850km assuming ~25km resolution data). The qualitative sensitivity analysis evaluated TempestExtremes filtered IVT data for AR characteristics such as AR life cycle coherence, thickness and length and tried to ensure that little-to-no equatorial blobs (i.e., tropical cyclones and/or storms associated with equatorial deep convection) were present in the filtered data to minimize the number of false positives in AR detection.

A novel extension to the TempestExtremes AR tracking algorithm was developed for this work to identify potential influences of domain size on the characteristics of ARs. This new algorithm takes the spatiotemporally stitched outputs from TempestExtremes to create a composite mask over the lifetime of each unique AR identified. The methods used in our algorithm share some commonality with other published methods including *Payne and Magnusdottir* [2014] and *Zhou et al.* [2018]. These composite masks are then used to find the latitudinal center-of-mass at each of several longitudinal cross-sections for each AR to generate the source-to-terminus pathways. Figure 2 shows an example of a single AR identified using the composite mask and center-of-mass approach and an entire DJF season worth of AR source-to-terminus pathways using one of the VR-CESM simulations. Once generated, these AR source-to-terminus pathways allow for the compilation of various summary statistics of the ARs. These summary statistics include:

(1) the number of unique ARs (total and western US landfalling)
(2) the lifetime of each unique AR (total and after western US landfall)
(3) the latitude and longitude of AR western US landfall location
(4) the average maximum IVT over the lifetime of the AR (total and after western US landfall)
(5) the duration of the AR (total and after western US landfall)
(6) the resultant *Ralph et al.* [2019] AR category for each AR that made landfall over the western US

3 Results

The goal of this work is to identify the extent to which the size of the refinement domain within a VR-CESM simulation can influence the simulated western US hydroclimate. To do this, we first examine if there are any discernible differences in the simu-

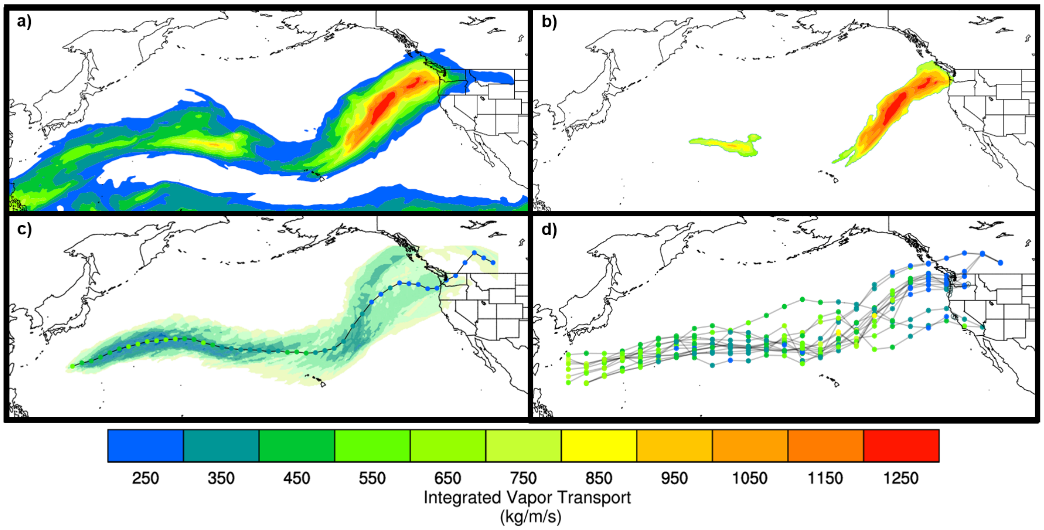

Figure 2. A step-by-step visual depiction of the TempestExtremes based workflow which takes a) 6-hourly integrated vapor transport (IVT) fields b) filters the fields into atmospheric river (AR) masks based on user selected parameter thresholds c) stitches and composites the AR tracks in time and space and d) compiles the AR source-to-terminus pathways and summary statistics over an entire DJF season. For a) and b), IVT magnitudes are shown for a particular 6-hourly time slice, whereas in c) and d) the maximum IVT over the lifetime of the AR is shown via circles at each longitude.

lations due to dynamical and/or thermodynamical properties of the atmosphere over the North Pacific Ocean. Next, we evaluate how these potential differences influence the atmospheric response to key climate modes of variability (e.g., the El Niño Southern Oscillation [ENSO]) and storm characteristics (e.g., ARs). Last, we examine how the characteristics of the western US hydroclimatology, particularly in mountainous regions, is shaped by the influence of refinement domain size. Throughout each of these analyses we focus on the boreal winter, specifically December, January, and February (DJF).

North Pacific Ocean Integrated Vapor Transport

IVT is a primary variable of interest for assessing how well models can simulate the western US hydroclimate [*Zhu and Newell*, 1998; *Ralph et al.*, 2006; *Neiman et al.*, 2008; *Ralph and Dettinger*, 2011; *Gimeno et al.*, 2014; *Lamjiri et al.*, 2018; *Shields et al.*, 2018]. As discussed by *Lavers et al.* [2016], IVT is a key driver of western US precipitation and has been shown to be easier to prognose than precipitation given that it is not as dependent on localized processes that shape precipitation intensity and spatial variability that

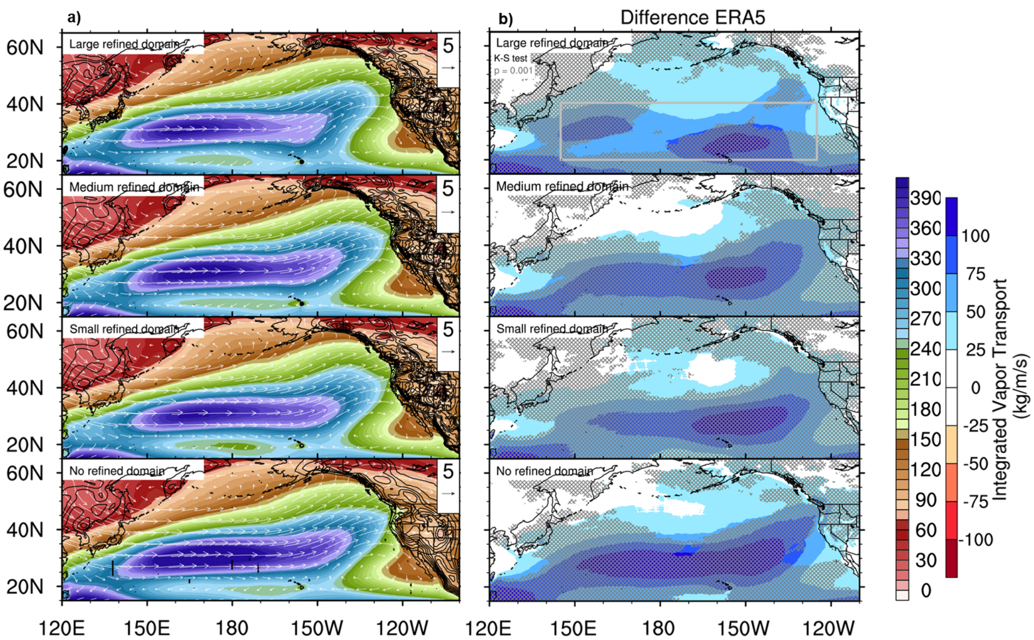

Figure 3. (a) DJF climatological average integrated vapor transport (IVT) for a uniform-resolution 1° CESM simulation (no refined domain) and three variable-resolution CESM cases with a 28km refinement domain that varies in extent longitudinally. Total wind vectors are overlaid along with 500m interval topography contours. (b) ERA5 differenced DJF climatological average IVT. The gray box region is used for analysis and spans across the three VR-CESM 28km refinement domains. The hatching overlay represents a statistically significant difference between ERA5 and CESM simulations (p-value = 0.001) using the Kolmogorov-Smirnov two-sample test (K-S test) adjusted using the *Benjamini and Hochberg* [1995] FDR (dark gray).

often need to be parameterized at the sub-grid-scale (e.g., convective precipitation due to frontal convergence and land-atmosphere feedbacks).

Total IVT is calculated as

$$IVT = \frac{1}{g} \int_{P_s}^{P_t} qV dp, \tag{1}$$

where g is the gravitational acceleration (9.8 m/s^2), P_s is the surface pressure level (Pa), P_t is the top of atmosphere pressure level (Pa), q is specific humidity (kg/kg), and V is the total wind (m/s; $\sqrt{u^2 + v^2}$ where u is the zonal wind component and v is the meridional wind component).

Figure 3a shows the IVT and total wind fields across CESM simulations for the DJF climatological period of 1985-2015. Figure 3b shows the difference in IVT over this same period from ERA5, where all IVT values with gray stitching are statistically significant at a p-value of 0.001 using the Kolmogorov-Smirnov two-sample test and further adjusted using the FDR. Interestingly, the magnitude of IVT bias generally decreases as the 28km refinement domain is expanded westward over the North Pacific Ocean. Across the box region highlighted in Figure 3b, all CESM simulation estimates of IVT are positively biased compared with the ERA5 dataset, however, the large refined domain has the lowest mean bias of +70 kg/m/s and the no refined domain has the highest mean bias of +87 kg/m/s. Notably, although the analysis is not shown, Kolmogrov-Smirnov significance testing of IVT differences between all CESM simulations at p-values of 0.001 and 0.01 (corrected using FDR) are not significantly different over most of the North Pacific and western US (save for the southern coast of Japan and a portion of the Northern Rockies in the large refined domain).

To understand why IVT increases as the longitudinal extent of the 28km refinement domain decreased over the North Pacific Ocean, we compare the water budgets of the VR-CESM simulations to the no refined domain. The water budget, similar to the technique used in *Dacre et al.* [2019], includes precipitable water, total precipitation (local sink), evaporation (local source), and zonal and meridional vapor transport (non-local source/sink) (Figure 4). We evaluate these water budget terms in the same region identified in Figure 3, which represents the core-region of IVT in DJF across the North Pacific. As shown by the precipitable water fields in Figure 4 the atmospheric column was drier in the large refined domain, particularly over the western equatorial Pacific Ocean. An indication of potential resolution-dependent processes that led to this drying of the atmo-

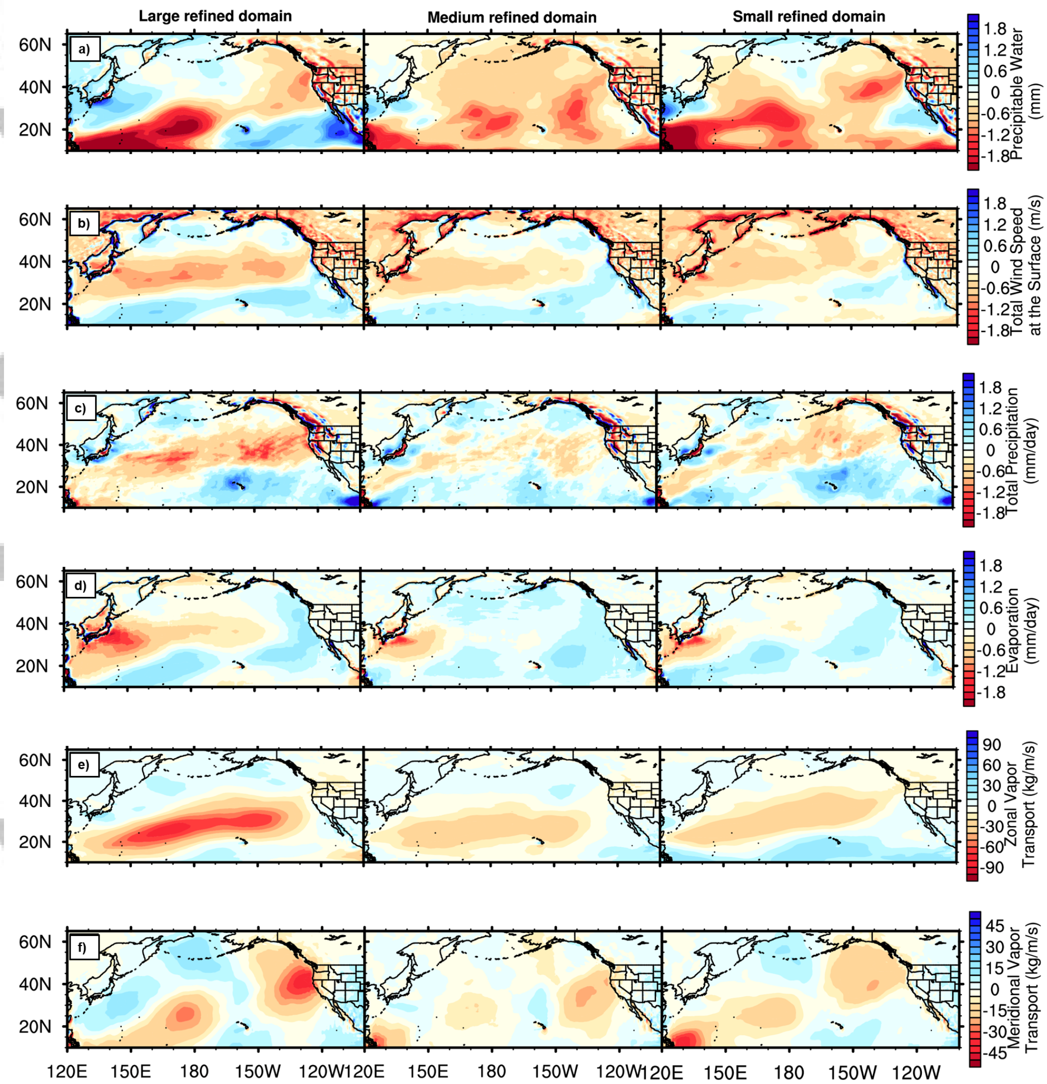

Figure 4. DJF climatological average difference in a) precipitable water b) total surface wind speed c) total precipitation, d) evaporation, e) zonal vaport transport, and f) meridional vapor transport compared against the no refined domain.

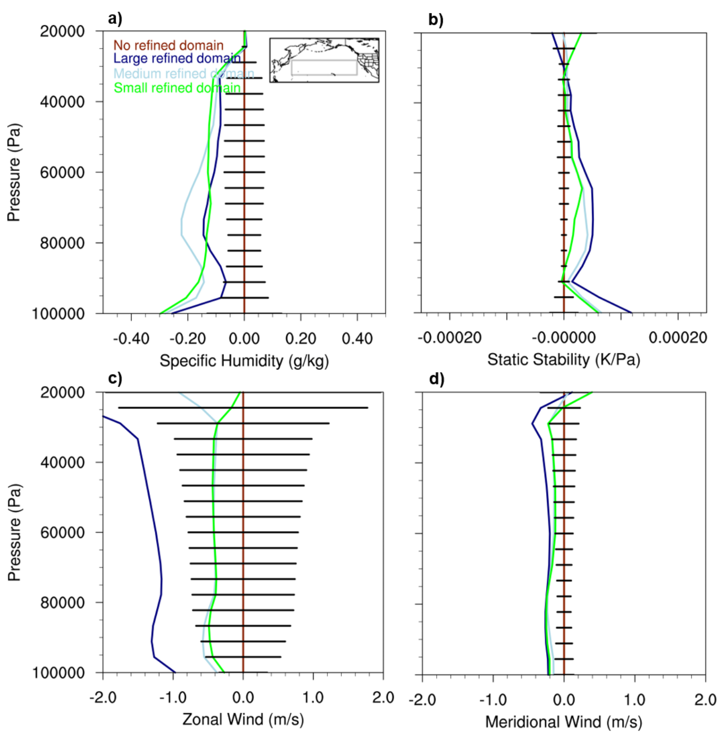

Figure 5. DJF climatological average vertical profile difference in a) specific humidity, b) static stability, c) zonal wind, and d) meridional wind against the no refined domain. Horizontal black bars represent the 95% confidence intervals based on DJF seasonal averages. The North Pacific Ocean box region over which the vertical profiles are generated is shown in the upper right corner of a).

spheric column is shown via the source terms in Figure 4 which highlight that as the longitudinal extent of the 28km refinement domain is extended westward towards the Asian coastline, surface wind speeds and evaporation are diminished, particularly off the coast of Japan and into the north-central Pacific where IVT is highest in Figure 3. Slower surface wind speeds combined with drier lower levels of the atmosphere in turn diminishes the water vapor available to be transported eastward and northward via the zonal and meridional vapor transport and, importantly, along one of the main source regions, southwest of Hawaii, and terminus regions, Pacific Northwest, of IVT. Figure 5 confirms this as the vertical profiles of the atmosphere across the North Pacific Ocean are more stable, drier, and the zonal wind speeds are dampened, particularly near the surface up to the region in which low-level jets usually occur within the warm-conveyor belt of North Pacific extratropical cyclones (i.e., ~1000-700 hPa, [*Dacre et al.*, 2019])

The net result of this dampened IVT is shown in Figure 4 where a westward expansion of the 28km refinement domain leads to less total precipitation throughout the North Pacific. This is shown primarily through a reduction in the contribution of convective precipitation to total precipitation and, interestingly, is not completely compensated for by a concomitant increase in stratiform precipitation (Supplemental Figure 1). The resolution dependence of convective precipitation is corroborated by other global and regional climate modeling literature [*Williamson*, 2008; *Bacmeister et al.*, 2014; *Zarzycki et al.*, 2014b; *O'Brien et al.*, 2016; *Rauscher et al.*, 2016; *Benedict et al.*, 2017; *Herrington and Reed*, 2017]. In some of these studies, precipitation fidelity is shown to improve with refinement of model resolution and is associated with an overall reduction in drizzle events (i.e., a decrease in the initiation of parameterized convective precipitation) along with an increase in extreme precipitation (i.e., precipitation intensity has been shown to scale with vertical velocity which is directly related with grid resolution in hydrostatic models). However, other studies evaluating multiple versions of CAM have shown that model simulated precipitation extremes at more refined resolutions (i.e., 0.25°) do not converge and even overshoot observations due to model adjustment changes (i.e., performance of model dynamics and physics at multiple resolutions) in intensity, duration, and/or frequency, potentially due to the cumulus parameterization and its allowance of overly saturated model columns too frequently [*Wehner et al.*, 2014; *Chen and Dai*, 2018]. More specifically, in a recent study by *Chen and Dai* [2019], CAM precipitation frequency and duration has been shown to decrease at coarser grid spacing, particularly for convective precipitation, and intensity increases at more refined grid spacing, especially for stratiform precipitation.

The decrease in western equatorial convective precipitation and meridional and zonal vapor transport (i.e., 120-170°E, 10-20°N) has an important influence on IVT over the North Pacific, particularly in regions in close proximity to Hawaii and off the coast of the Pacific Northwest. This indicates that refinement domain size may have also had an influence on the atmospheric response at sub-seasonal scales through the Madden Julian Oscillation (MJO) and at inter-annual scales through the El Niño Southern Oscillation (ENSO). Although a comprehensive analysis of sub-seasonal scale phenomena is out-of-scope for this climate sensitivity study, we note a few of the important atmosphere-ocean couplings given their importance to western US hydroclimate. At sub-seasonal timescales, the region southwest of Hawaii has been shown to be a source region of IVT to the western US through its association with the Madden Julian Oscillation (MJO), or eastward migration of equatorial convection, during the northern hemisphere winter season. As shown by *Guan et al.* [2012] and *Zhou et al.* [2018], MJO phases can be directly linked to IVT anomalies which in turn have a particular influence on the strength and variability of wintertime ARs that make landfall in the western US (e.g., MJO Phase 6-7 increase both the number and lifetime of AR events over the North Pacific). Supplemental Figure 1 shows how refinement domain size has a direct influence on the convective precipitation in the simulations, particularly equatorial deep convection, which may be an indication that the representation of particular phases of MJO and, consequently, anomalous IVT were also dependent on refinement domain size. Meridional vapor transport may also have been impacted by other sub-seasonal atmosphere-ocean feedbacks that led to the inhibition of local evaporation in the East China Sea and Sea of Japan such as the East Asian Cold Surge (EACS) associated with southerly movement of polar air masses [*Jiang and Deng*, 2011]. Supplemental Figure 3 compares the surface sensible and latent heat fluxes and minimum and maximum surface temperatures across simulations. A general warming of Siberia and Northern China occurs as the 28km refinement domain is expanded westward which, as shown by surface sensible and latent heat fluxes, would act to suppress the seasonal strength of EACS events as they move into the Sea of Japan and East China Sea. This regional warming could be a response to a strengthening of the Siberian High which in turn would augment the prevalence of onshore (relatively warm, moist) or offshore (relatively cold, dry) winds due to sharper gradients in land-sea contrast at more refined resolution [*Kumar et al.*, 2019]. Diminished EACS would in turn minimize the sub-seasonal atmospheric disturbances that are induced by these events which would feedback onto the North Pacific trough-ridge patterns and, inevitably, dampen IVT. These two sub-seasonal processes would make for interesting avenues to explore in future research using these VR-CESM domain sensitivity experiments.

Representation of the Extreme 1998 El Niño

The El Niño Southern Oscillation (ENSO) is a coupled ocean-atmosphere interaction, which alternates between its positive phase (El Niño) and its negative phase (La Niña) every 2-7 years [*Philander*, 1985; *Neelin et al.*, 1998; *McPhaden et al.*, 2006]. ENSO accounts for the largest fraction of inter-annual climate variability and alters global circulation and weather patterns around the world via an atmospheric bridge, or teleconnection [*Rasmusson and Wallace*, 1983; *Alexander et al.*, 2002]. During El Niño, anomalous oceanic heat builds up in the tropical east-Pacific as a result of slackening tradewinds associated with a weakened Walker circulation, downwelling oceanic Kelvin waves, and a deepening thermocline [*Neelin et al.*, 1998; *Timmermann et al.*, 2018]. This in turn, alters the zonal temperature gradient of the tropical Pacific exciting deep convection far out into the east-Pacific, where the climatologically cool sea surface temperatures (SSTs) would normally prevent deep convection from occurring [*Hoerling et al.*, 1997; *Sabin et al.*, 2013]. The anomalous convection excites a quasi-stationary Rossby wave that deepens the Aleutian low and moves its center of action to the East [*Bjerknes*, 1969; *Hoskins and Karoly*, 1981; *Rasmusson and Wallace*, 1983; *Trenberth et al.*, 1998]. This has the effect of strengthening and extending the North Pacific stormtrack and moving it south resulting in enhanced western US precipitation, and in particular, for California [*Trenberth et al.*, 1998; *Cayan et al.*, 1999; *Feldl and Roe*, 2011; *O'Brien et al.*, 2019; *Patricola et al.*, 2019].

Given that El Niño's primary region of action is across the eastern Pacific, it is reasonable to suspect that there may be sensitivity to the longitudinal extent of the VR-CESM refinement domain in the representation of the El Niño tropical Pacific - North-east Pacific teleconnection and resultant precipitation response across the western US. For this analysis we focus on the DJF precipitation response to El Niño in California as the transpacific teleconnection signal tends to be the largest here among all regions across the western US [*Cayan et al.*, 1999; *Feldl and Roe*, 2011; *Patricola et al.*, 2019]. The VR-

CESM simulations span December 1986 through February 2014, thus simulating the extreme El Niño year of 1998, where California received near record levels of precipitation and sustained significant infrastructure and property damage resulting in large financial losses due to the widespread flooding that occurred that year [*Hoell et al.*, 2016; *Lee et al.*, 2018; *Corringham and Cayan*, 2019]. That the physical driver of the El Niño teleconnection to California is tropical deep convection, which transmits energy north and east across the Pacific, the placement and extent of the refined grids makes its representation in the VR-CESM simulations important for understanding domain size sensitivity. Supplemental Figure 2 shows the 1998 DJF tropical east-Pacific SST anomaly with the four CESM grids overlain. Additionally, the dot in each panel represents the estimated 1998 DJF average center of deep convection as indicated by the ENSO Longitude Index [*Williams and Patricola*, 2018] and the gray box indicates the more conventional Niño3.4 region.

The results of any single initialized simulation are subject to variability introduced by its unique initial conditions and subsequent evolution in time. Thus, the atmospheric response to the 1998 El Niño and associated precipitation response in California in each of the three refined domain experiments represents a single outcome of a range of plausible outcomes. Therefore, to isolate the El Niño forced response in each of the three refined domains we ran 10 additional perturbed initial condition simulations of 1998 at each domain extent. This is done to account for internal variability and isolate the signal-to-noise of the effect of refinement domain extent. Given the large computational costs of running multi-member ensembles of global simulations we chose 10 ensemble members for 1998 following from *Deser et al.* [2012, in press 2019] (plus the simulation of 1998 in the climatological runs).

As a benchmark by which to compare the VR-CESM domain sensitivity simulations, we use both a large-ensemble of 1° resolution global atmospheric model (CAM5.1) simulations and a reanalysis (ERA5). The CAM simulations make up a 50 member large-ensemble extending from 1959-2018 and are, similar to the VR-CESM simulations, of the AMIP class where each member is forced by the observed SSTs and radiative forcings, but differentiated by slight perturbations in their initial conditions. The CAM simulations are part of the Climate of the Twentieth Century (C20C) Project and are a subset of a larger multi-model ensemble [*Folland et al.*, 2014; *Stone et al.*, 2019]. Additionally, we employ the ERA5 reanalysis product as the ground truth representation of California DJF precipitation climatology and the 1998 El Niño response [*Copernicus Climate Change Service (C3S)*, 2017].

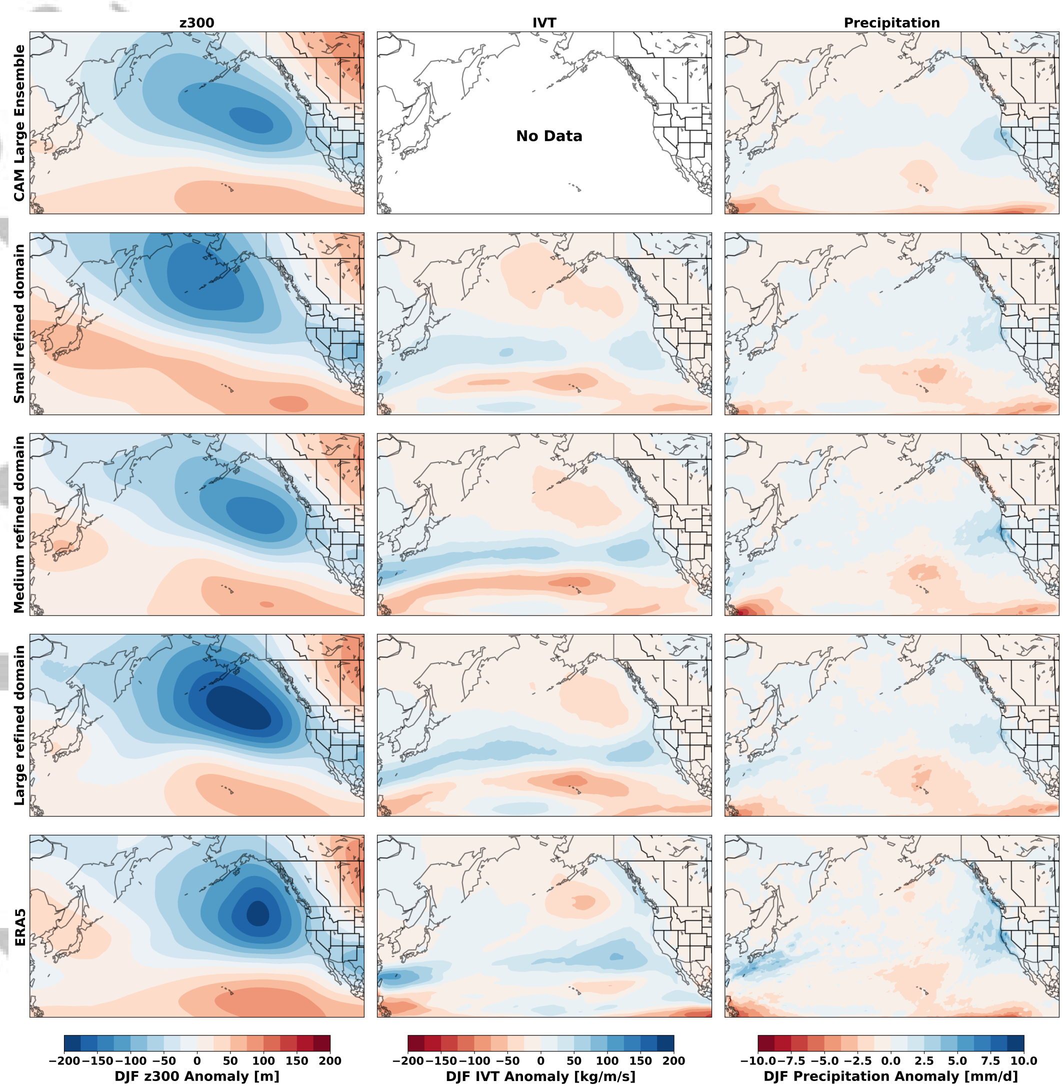

Figure 6. The ensemble mean representation of the extreme 1998 El Niño among three key atmospheric variables: left column, the 300-hPa geopotential height anomaly; center column, the Integrated Vapor Transport (IVT) anomaly; and right column, the precipitation anomaly. Each variable is represented by a different model product in each row: top row, the uniform 1° resolution of the CAM large ensemble; top middle row, the small refined domain ensemble; middle row, the medium refined domain ensemble; bottom middle row, the large refined domain ensemble; and bottom row, ERA5 reanalysis. The ensemble means are comprised of 50 and 11 simulations of 1998 for the CAM and the three VR-CESM domain experiments respectively. Anomalies are calculated with respect to the all-year DJF climatologies for each simulation.

Figure 6 shows the representation of the strong 1998 El Niño event among several key variables. In the left column, the geopotential height anomaly at 300-hPa, the center column shows the IVT anomaly, and the right column shows the precipitation anomaly all corresponding to their respective DJF climatologies. The top row shows the ensemble mean anomalies of 50 simulations of 1998 from the uniform 1° CAM large ensemble, while the top center, middle center, and bottom center rows show the ensemble mean anomalies of 11 simulations of 1998 for each VR domain experiment. We were unable to calculate the IVT field for the CAM ensemble as the 3D specific humidity variable was not output for this experiment. The broad similarities of the geopotential height anomalies across the different VR-CESM domains are consistent with the atmospheric response to El Niño ocean forcing, in particular, the deepening of the Aleutian Low [*Bjerknes*, 1969; *Hoskins and Karoly*, 1981; *Rasmusson and Wallace*, 1983; *Trenberth et al.*, 1998]. However, each model experiment has its own unique character and differ in their respective representations of the atmospheric response to El Niño. For example, relative to ERA5, the center of z300 height anomaly is moved further to the Northwest in the small refined domain, whereas in the CAM simulations and the medium/large refined domains the location is approximately correct, however the response is weaker/stronger than what is observed in ERA5. Similarly with IVT (Figure 6 middle column), the small refined domain simulates a stormtrack that is most inconsistent with ERA5 while the medium and large refined domains broadly simulate the correct strength and position. The precipitation response shows the most heterogeneity across simulations (Figure 6 right column) likely reflecting model sensitivity to the complexity of processes and parameterizations necessary to generate precipitation. In terms of the spatial footprint of the western US precipitation anomaly in each simulation, the CAM large ensemble simulations and the medium refined domain most closely match ERA5. Though it is notable that both the CAM large ensemble simulations and all of the refined domain simulations fail to capture the precipitation near Washington State and British Columbia. In the refined domain experiment that best simulates precipitation in California, the medium refined domain, the effect of the increased resolution is apparent relative to the uniform 1° resolution in the CAM large ensemble simulations. This is likely because the refined domain simulations better resolve orthographically enhanced precipitation in the Sierra Nevada mountains.

Figure 7 panel (a) shows that the distribution of the 1998 CAM simulations (red) clearly separate from the climatological distribution (black) indicating a clear and strong

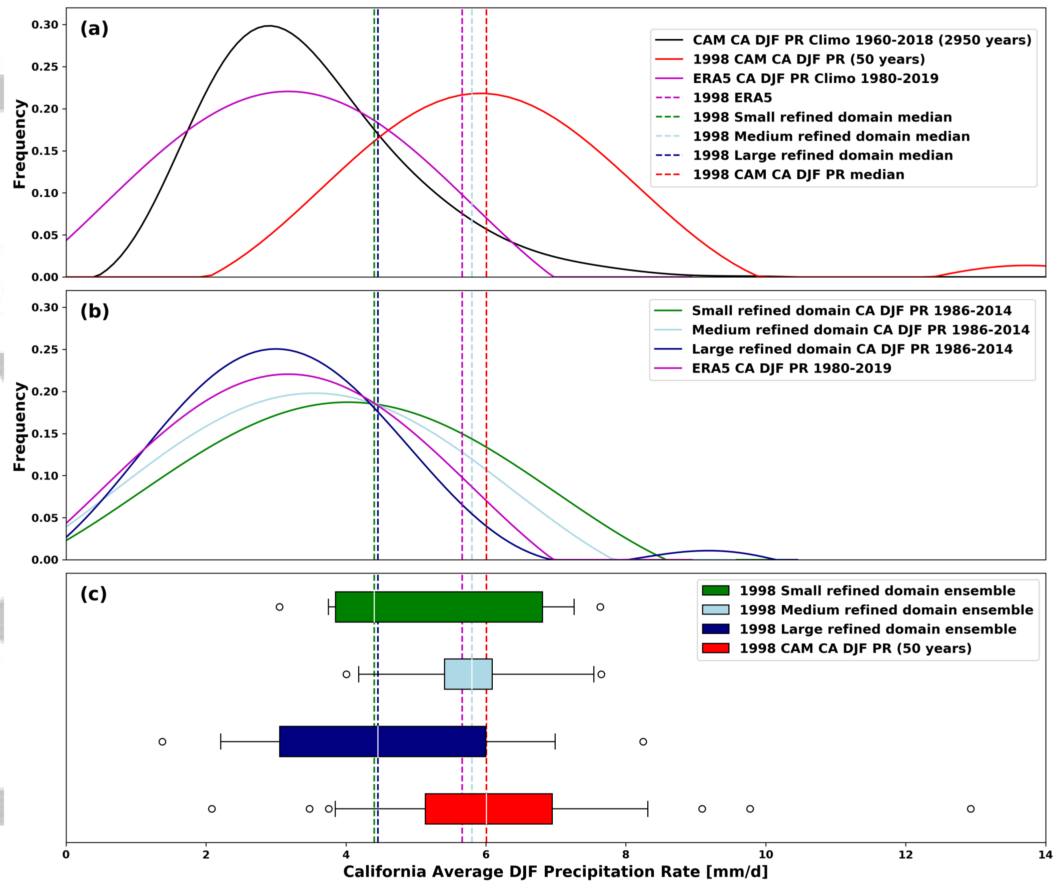

Figure 7. Probability Density Functions (PDFs) of the California DJF spatiotemporal average precipitation rate. Panel (a) corresponds to the CAM large ensemble all-year DJF climatology (black curve) and the 50 member ensemble representation of the extreme 1998 El Niño year (red). Panel (b) shows the DJF climatologies of the three different VR-CESM simulations. Both panels (a) and (b) have the ERA5 climatology overlain (magenta). Panel (c) shows box and whisker plots of the ensemble of 1998 simulations for each VR-CESM experiment. Box edges indicate the 25th/75th percentiles and the whiskers indicate the 5th/95th percentiles with outlier points plotted beyond the whiskers. For reference, each panel has a vertical dashed line to indicate the ensemble median for each experiment and the single year representation derived from ERA5.

ocean forced response from the extreme El Niño. Moreover, relative to the ERA climatology (magenta), the CAM ensemble accurately captures California's DJF climatological precipitation (black) albeit with more refined tails due to greater sampling of internal variability. Within a small margin of error, the ensemble median of the 1998 CAM simulations accurately captures the outcome of the 1998 El Niño precipitation response in California indicated by the proximity of vertical dashed red and magenta lines. We note here that throughout Figure 7 medians rather than means are shown only to be consistent with the standard interpretation of box and whisker plots, however, the normality of the distributions ensures that results are not sensitive to whether means or medians are used to show ensemble averages. Additionally, it is notable that the 50 member ensemble of CAM simulations for the 1998 El Niño include both members that fall far below (near the climatological mean) and far above the 1998 response estimated by ERA5. This clearly demonstrates that any single initialized simulation may result in a wide range of simulated outcomes for the same event and that it is only with an ensemble of perturbed initial condition simulations that the true forced response can be separated from internal variability [*Deser et al.*, 2012, 2016, in press 2019]. However, the ensemble median of the 50 simulations of 1998 provides a close approximation of the response estimated by ERA5 indicating that the DJF precipitation 1998 in California was indeed primarily the result of large-scale ocean forcing. Panel (b) shows that the DJF precipitation climatologies of all VR-CESM domain sizes are roughly the same, suggesting that the representation of average California DJF precipitation is not sensitive to domain refinement extent. In the ERA5 data, the extreme El Niño of 1998 occupies the 95$^{\text{th}}$ percentile of the distribution. Only in the CAM simulations and the medium refined domain experiment does the 1998 ensemble median occupy approximately the correct percentile of the climatological distribution. Notably, both the small and large refined domain ensemble median simulates a much weaker representation of the extreme 1998 El Niño (falling closer to the climatological mean). However, that said, panel (c) shows the box and whisker plots for the 10 member ensemble of simulations of the extreme 1998 El Niño and each experiment spans the range of internal variability as indicated by the CAM large ensemble. Therefore, from a statistical perspective, we cannot say that one domain extent represents El Niño better than another. Despite this null result, the lack of sensitivity of the El Niño teleconnection to western US precipitation is still important in that it appears that a large refined domain may not be required to ensure simulation precipitation fidelity in the western US. Thus, computational resources can be focused elsewhere such as longer duration simulations and/or more ensemble members.

Western US Landfalling Atmospheric Rivers

As discussed in *Gimeno et al.* [2014], and in more detail in *Ralph and Dettinger* [2011] and *Jiang and Deng* [2011], the aforementioned dynamical and thermodynamical differences induced by refinement domain size across CESM simulations likely influenced the most extreme form of IVT, ARs. Furthermore, *Hagos et al.* [2015] posited that although their MPAS simulated estimates of AR counts in the North Pacific did not show strong dependence on resolution, that AR position at landfall and associated precipitation may have been influenced. Given these assumptions, we evaluate the impact of the 28km refinement domain extent on the characteristics of ARs prior to and after western US landfall. We employ the *Ullrich and Zarzycki* [2017] TempestExtremes AR detection algorithm along with a novel AR lifecycle stitching algorithm developed specifically for this study. Table 2 gives an overview of the various summary statistics of AR characteristics over the 1985-2015 DJF climatology. Summary statistics were compiled by using the AR tracking algorithms to filter individual AR events for each DJF season, averaging these individual statistics across a given DJF season, and then compiling each DJF season into a climatology and providing a 95% confidence interval based on the seasonal averages. The AR metrics evaluated include: the total number of ARs identified, the number of ARs that made landfall in the western US, the average latitude and duration of the AR after landfall, the maximum IVT identified over the lifetime of the AR after landfall, and, finally, the *Ralph et al.* [2019] AR category scale.

The total number of annual ARs have been identified in several studies to date using various satellite and/or reanalysis datasets. *Waliser et al.* [2012] found that a typical AR count over the North Pacific ranged between 122 to 137 per year over a two-year period using IWV derived from the Atmospheric Infrared Sounder observations from the NASA Aqua satellite. *Payne and Magnusdottir* [2014] showed a higher estimate in AR counts over the North Pacific of 156 per year from 1979-2011 using the MERRA reanalysis product, although, importantly, daily extreme precipitation has been shown to be quite different in MERRA versus other global precipitation products [*Sun et al.*, 2018]). Importantly, AR count can depend on the detection method used [*Shields et al.*, 2018]. Using TempestExtremes, we find a comparable AR count over our 30-year period of 1985-2015 of 133 per year when we use the ERA5 dataset. As indicated previously, each of the CESM simulations had higher IVT than ERA5 and, not surprisingly, this resulted in a higher number of total ARs identified (Figure 3). This AR count varied from 139 per year (large refined domain) to 141 per year (small refined domain). However, for DJF, both ERA5 and all of the CESM simulations show comparable seasonal AR count statistics with overlapping counts at the 95% confidence interval (Table 2).

Although total AR counts are relevant in identifying if CESM is simulating the various dynamical and thermodynamical processes that seed and propogate ARs over the North Pacific, water managers in the western US are primarily interested in the number of ARs that make landfall due to their role as both a boon and bane on reservoir management [*Ralph et al.*, 2006; *Vano et al.*, 2019]. To estimate AR landfall counts, *Neiman et al.* [2008] used 8-years of Special Sensor Microwave Imager observations to identify that ARs made landfall in 27-49 (10-19) days per year in Oregon/Washington (California). *Payne and Magnusdottir* [2014] identified that there were an average of 6, 5, and 3 AR landfall dates in the months of DJF (14 total), respectively, with 749 out of the 4992 total dates (15%) associated with landfalling ARs. Our estimates of DJF landfalling ARs in ERA5 are similar, yet slightly higher (17), compared with those in *Payne and Magnusdottir* [2014]. Interestingly, all CESM simulations overestimate the number of ARs that make landfall save for the large refined domain, 20, at the 95% confidence interval. Regardless of differences in landfalling AR counts, the average latitude in which they make landfall are agreed upon between CESM simulations and ERA5 (41 N near the California/Oregon border).

In addition to the number of landfalling ARs, it's also necessary to quantify the duration and magnitude of these events, as both are important for assessing impacts [*Ralph et al.*, 2019]. For example, *Ralph et al.* [2013] showed that landfalling ARs over California typically have durations of 20 hours, but can last up to 40 hours in extreme cases. Our evaluation of the ERA5 dataset complements this finding and shows that the average duration of the AR events identified in DJF last 18 hours (Table 2). Interestingly, CESM model simulated ARs on average last 6-12 hours longer than those found in the ERA5 dataset. This is likely related to the fact that the average max IVT is also ~80-100 kg/m/s higher in CESM simulations than in the ERA5 dataset. The result of this high bias in IVT is that CESM simulations have a concomitant increase in *Ralph et al.* [2019] scores during DJF (2.38-2.47) compared with ERA5 (1.83). Albeit only a difference of 1 category in the *Ralph et al.* [2019] scale, the qualitative difference between category 1 versus category 2 is the difference between ARs being primarily beneficial to water resources versus beginning to pose some type of hazard.

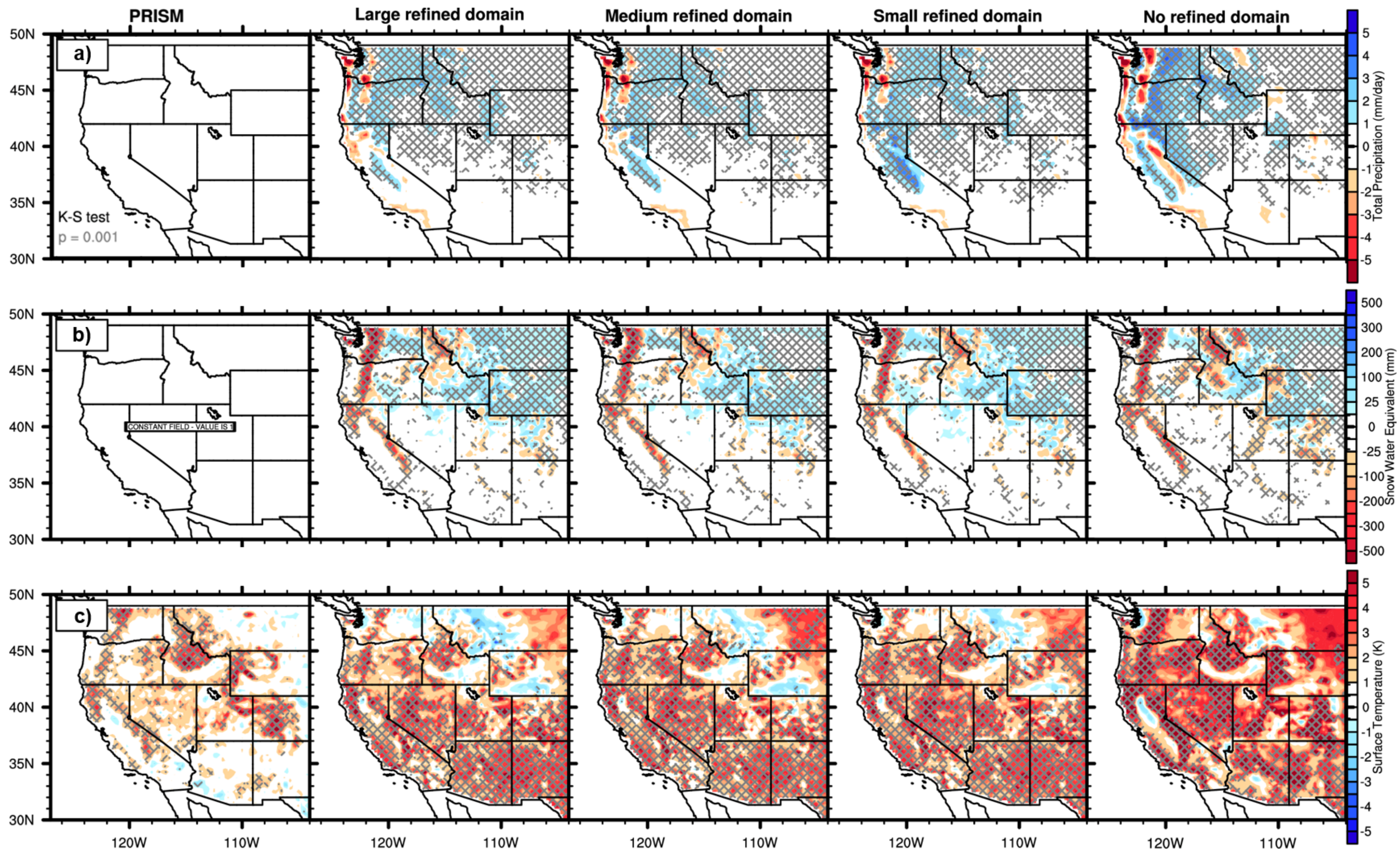

Figure 8. DJF climatological average a) total precipitation, b) snow water equivalent, and c) surface temperature for a uniform-resolution 1° resolution CESM simulation (no refined domain) and three variable-resolution CESM cases (large refined domain, medium refined domain, and small refined domain) differenced against the L15 reanalysis dataset. For comparison, the PRISM reanalysis dataset is shown in the left most column. The hatching overlay represents a p-value exceedance of 0.001 (dark gray) using the Kolmogorov-Smirnov two-sample test (K-S test) adjusted using the *Benjamini and Hochberg* [1995] False Discovery Rate and compared with L15.

Table 2. DJF climatological average summary statistics for western US landfalling ARs over the years 1985-2015 with 95% confidence intervals. In the landfalling ARs column, emboldened numbers represent the percentage of landfalling ARs relative to the total number of ARs.

Dataset Name	*Total ARs*	*Landfalling ARs*	*Average Latitude*	*Average Duration (days)*	*Average Maximum IVT (kg/m/s)*	*Average Ralph et al. 2019 AR category*
ERA5	37±1	17±2 (**46%**)	41.6±0.68	0.76±0.11	746±28.1	1.83±0.16
Large refined domain	35±2	20±2 (**57%**)	41.4±0.83	1.26±0.19	842±32.4	2.44±0.20
Medium refined domain	35±1	22±1 (**63%**)	41.3±0.66	1.13±0.12	830±22.8	2.38±0.14
Small refined domain	36±2	22±1 (**61%**)	41.1±0.76	1.23±0.19	842±28.1	2.47±0.20
No refined domain	34±1	21±2 (**62%**)	41.4±0.84	1.20±0.15	824±26.1	2.44±0.19

Western US Mountain Hydroclimate: Precipitation, Snowpack, and Surface Temperature

The differences in AR landfall counts between the large refined domain and the other CESM simulations likely played a role in shaping the precipitation totals in the western US. To explore this we compare the DJF hydroclimatology (i.e, total precipitation, snow water equivalent, and surface temperature) between the CESM simulations and two widely used reanalysis products, L15 and PRISM (Figure 8). Across the western US, CESM simulations are generally positively-biased in total precipitation and surface temperature and negatively-biased in snow water equivalent when compared against L15. The large refined domain simulated the DJF climatology most closely with L15 with total precipitation at +0.3 mm/day, snow water equivalent at -5.3 mm, and surface temperature at +2.3 K, whereas the no refined domain was least similar with total precipitation at +0.5 mm/day, snow water equivalent at -16 mm, and surface temperature at +3.3 K. Therefore, all VR-CESM simulations outperform the uniform-resolution 1° resolution simulation. This highlights the added value of high-resolution modeling over the western U.S. compared with conventional GCM simulations (e.g., better representation of complex terrain and land-surface cover). However, in concert with the positively-biased surface temperatures, which likely altered general storm precipitation phasing from snowfall to rainfall too regularly, in CESM simulations it appears that 28 km resolution was insufficient in representing the various topographic dependent processes in the Oregon and Washington Cascades. This is shown by the clear negative-bias in total precipitation and snow water equivalent throughout much of the Cascades which consists of a chain of highly localized and intermittent volcanic peaks.

Across the VR-CESM simulations there are important regional differences, particularly in the coastal ranges of the western US, that are likely related to refinement domain size. The impact of refinement domain size is indicated most clearly in California. As shown for the California Central Valley and Sierra Nevada, the large refined domain provides the best skill in representing the expected total precipitation climatology of L15 and PRISM, whereas the small refined domain is high-biased with statistically significant errors across most of the central-to-northern portions of California. This is likely because of better IVT representation in the large refined domain over the North Pacific (Figure 3). In terms of precipitation phasing, all VR-CESM simulations are significantly low-biased in their DJF climatology of snow water equivalent compared with the reanalyses datasets, akin to other regions of the western US. This lack of DJF snow water equivalent is insensitive to refinement domain size and is more likely related to the overall warm-bias in CLM5.0-SP simulated surface temperatures. The warm-bias is important because a discrete range of surface temperatures dictate precipitation phase partitioning (i.e., +2 C [all rain] ≥ 0 C [mixture of rain-snow] ≥ -2 C [all snow]) and ripening, or changes in density and albedo, of the snowpack over the water year in CLM5.0-SP [*Lawrence et al.*, 2019]. Interestingly, surface temperature biases appear to be dictated more by minimum than maximum surface temperatures (Supplemental Figure 4). As noted before, *Walton and Hall* [2018] has shown that L15 surface temperatures are likely at the lower end of reanalysis dataset estimates, due to fixed assumptions in lapse-rates, and this is confirmed with the DJF climatology comparison with PRISM indicating that surface temperature biases may be inflated when comparing simulation results to L15. Regardless of assumptions in L15, comparisons with PRISM indicate that there is a systematic warming and over correction of previously identified surface temperature biases across the western US when CESM simulations with CAM5.4-SE are run with CLM4.0-SP versus CLM5.0-SP [*Rhoades et al.*, 2018b] with deleterious impacts on seasonal dynamics of mountain snowpack. Previous VR-CESM simulations using CAM5.4-SE coupled with CLM4.0-SP showed much better agreement with observational estimates of western US mountain snowpack.

To expand our analysis beyond DJF and explore how refinement domain size may have influenced the accumulation and melt seasons in western US mountains we present daily climatologies across the water year (Figure 9). Similar to the DJF climatologies, VR-CESM simulations perform well for accumulated total precipitation in western US mountains with all VR-CESM simulations falling inside of the 95% confidence intervals of L15 throughout the entire water year. Accumulated total precipitation is slightly low-biased in the large refined domain and the medium refined domain (-9 to -34 mm) and high-biased in the small refined domain (+28 mm) across western US mountain ranges. The mountain region with most disagreement across VR-CESM simulations is the California Sierra Nevada where the large refined domain has a bias of -144 mm and the small refined domain has a bias of +87 mm (both within ~10% of L15; Supplemental Figure 5). This is likely related to the previously mentioned difference in AR landfall counts of 2 per DJF, associated with refinement domain size (Table 2). Although, total precipitation is generally well represented across VR-CESM simulations, daily snow water equivalent is low-biased across all VR-CESM simulations. Peak snow water equivalent estimates are low biased by -68 to -75 mm across the western US mountains in all VR-CESM simulations. With that said, all VR-CESM simulations still outperform peak snow water equivalent estimates provided by the uniform 1° resolution CESM simulation (-124 mm bias). Further, although coastal mountains show poor snow water equivalent simulation performance across VR-CESM simulations the interior mountain ranges are better simulated (Supplemental Figure 5). For example, in the Rockies peak snow water equivalent estimates are low biased by -18 to -28 mm (within ~15% of L15). Regardless of mountain range, VR-CESM simulations using CLM5.0-SP still exhibit a systematic bias whereby snow water equivalent peaks too early and melts too fast, an holdover identified in previous VR-CESM studies using CAM5.4-SE coupled with CLM4.0-SP over the western US [*Rhoades et al.*, 2016, 2018a,b].

As mentioned previously, the warm-bias in surface temperature was likely the major reason for the deleterious impacts on seasonal mountain snowpack. VR-CESM simulated surface temperatures are biased between +2.9 and +3.0 (+1.6 to +1.7) K on average throughout the water year when compared with L15 (PRISM). This warm-bias is

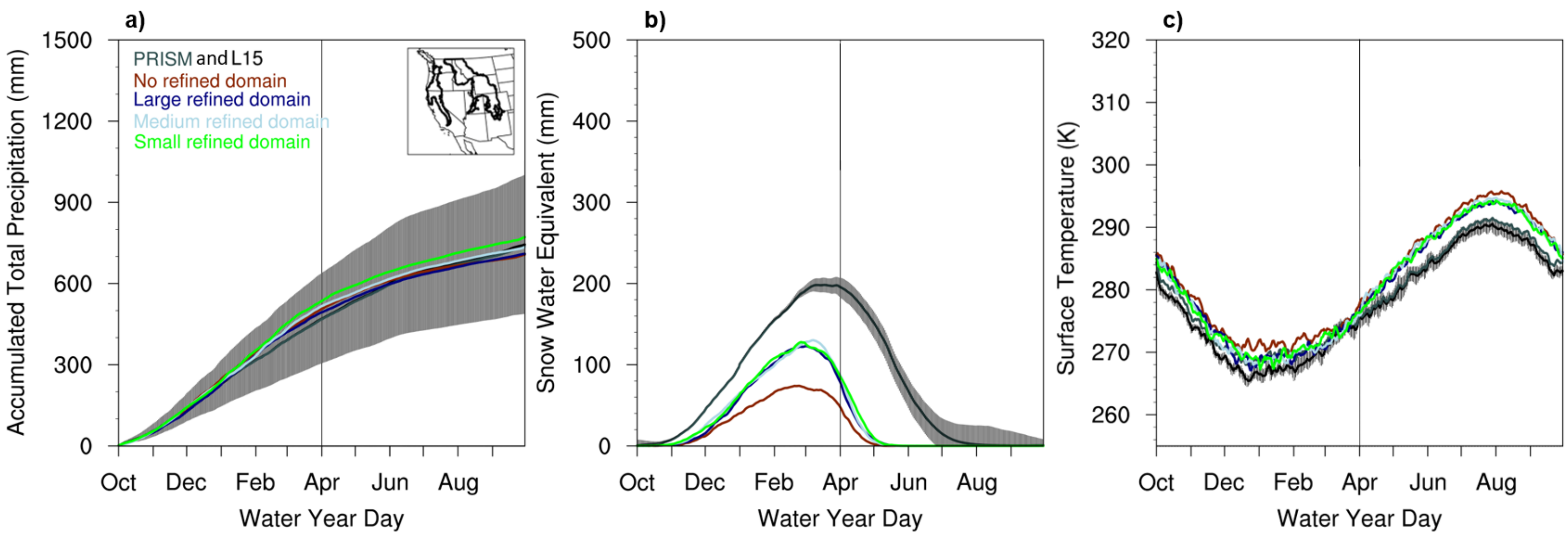

Figure 9. Western US mountain daily climatological average a) accumulated total precipitation, b) snow water equivalent, and c) surface temperature for each of the CESM simulations, no refined domain (red), large refined domain (navy blue), medium refined domain (light blue), and small refined domain (green), compared with the L15 reanalysis dataset (black). For comparison, the PRISM reanalysis dataset (gray) is also shown. The vertical black lines overlaid onto the L15 curves represent the 95% confidence interval based on daily average values.

pronounced and is particularly impactful in the accumulation season where precipitation is unable to change its phase from rain to snow and/or preserve at the land-surface and in the melt season where the snowpack ripens too quickly (i.e., snow density increases too fast) lowering the albedo which leads to earlier spring-season melt [*Colombo et al.*, 2019]. Supplemental Figure 6 shows this by highlighting the frost (Tmin < 273K), freezing (Tavg < 273K), and ice day (Tmax < 273K) deficits across CESM simulations, the naming conventions are consistent with the World Meteorological Organization [*Contosta et al.*, 2019]. Freezing days are a proxy for the days available to accumulate snowfall at the surface and frost days are a proxy for the number of days in which snow can be preserved into late-winter to early-spring. VR-CESM freezing day deficits range from -12 to -24 days with the uniform-resolution 1° simulation having the largest freezing day deficit of -43 days. This 2-3 week freezing day deficit in early-winter inhibits the VR-CESM simulations from allowing precipitation events to precipitate as snowfall and accumulate as snowpack (and is most pronounced in the coastal mountain ranges). In late-winter to early-spring, VR-CESM simulations have another 2-3 week frost day deficit which forces the snowpack to ripen and melt more abruptly than is expected in L15. Therefore, it appears that none of the snow-process enhancements in CLM5.0-SP could compensate for these surface temperature biases including the new upper limit of snow water equivalent (10,000 mm), the updated partitioning of snow cover fraction (depletion) curves for the snow accumulation (melt) seasons, and/or the new snow density parameterization that now depends on both temperature and wind, to account for wind-driven snow compaction [*van Kampenhout et al.*, 2017]. Of note, *Rhoades et al.* [2018c] and *Rhoades et al.* [2018d] have shown that these systemic snow water equivalent lifecycle biases are prevalent in other global and regional climate models of comparable and/or refined model resolutions too, particularly in the melt season. This was similarly confirmed in *Xu et al.* [2019] who devised an error decomposition framework to quantitatively show that simulated SWE biases in regional climate models are resolution-dependent, however are also related to biases, that can sometimes offset, in the spatial and elevational distribution of precipitation (i.e., microphysics scheme), lapse-rates (i.e., boundary layer scheme), and rain-snow partitioning in the land-surface model (i.e., surface temperature threshold choice). Future work should evaluate this systematic increase in surface temperature from CLM4.0-SP to CLM5.0-SP. A hypothesis as to why a general warming occurred is due to several new modifications to soil evaporation and/or transpiration in CLM4.0-SP versus CLM5.0-SP. More specifically, CLM5.0-SP soil evaporation now includes a resistance parameterization and transpiration includes a hydraulic stress parameterization. These two modifications likely led to drier soil and vegetation and enhanced the surface sensible heat flux, but need to be more robustly explored using an error decomposition framework mentioned previously and/or energy budget analysis to confirm this hypothesis.

4 Discussion and Conclusions

The effects of refinement domain size on simulation fidelity in the RCM literature has been extensively explored, however this same analysis has not been methodically tested in the VRGCM literature. Therefore, the goal of this study was to identify if the refinement domain size in VR-CESM had a significant impact on the simulated dynamical and thermodynamical characteristics of the atmosphere over the North Pacific Ocean and, if so, what were the concomitant impacts on the simulated hydroclimatology over the western US.

We found that the westward expansion of the 28km refinement domain over the North Pacific Ocean led to a decrease in IVT in DJF resulting in a closer approximation to ERA5. Lower DJF IVT can be attributed to the atmosphere becoming more stable, drier, and less windy near the surface. In turn, lower simulated DJF IVT led to a decrease in total precipitation. Interestingly, refinement domain size (or more refined resolution in general) did not have a significant impact on the total count of DJF ARs, but does seem to reduce the number of landfalling ARs, specifically in California. The lower number of landfalling ARs was shown to improve DJF precipitation in the western US, but was mostly evident over California. At inter-annual timescales, the simulated atmospheric response to strong El Niño events does not seem to be influenced by refinement domain size.

Regardless of 28km refinement domain size over the North Pacific Ocean, we found that DJF simulated IVT is high-biased across all CESM simulations when compared against ERA5. The high-bias in IVT resulted in landfalling ARs that are generally too strong according to the *Ralph et al.* [2019] scale (i.e., max IVT is too high and AR duration is too long). Although DJF total precipitation was better simulated with the westward expansion of the 28km refinement domain, snow water equivalent was low-biased throughout most of the western US, save for the interior mountain ranges. The low-bias in snow water equivalent in the VR-CESM simulations is intuitive as topographic resolution was still too coarse to properly represent certain western US mountain ranges, in particular the intermittent and localized peaks of the Cascades and sharp elevation gradients of the eastern Sierra Nevada. However, even when comparing 28km resolution VR-CESM simulations using CLM4.0-SP in past studies to the simulations using CLM5.0-SP in this study, a systematic increase in surface temperature was evident. This systematic increase in surface temperature altered precipitation phase partitioning and overall residence time of snowpack in the mountains.

Therefore, although the DJF simulated climatology across the VR-CESM simulations did produce some differences, particularly in North Pacific IVT, minimal differences were actually seen on AR characteristics and resultant influences on the simulated western US hydroclimate, save for precipitation over California. Topographic resolution and/or the version of land-surface model used appears to be more of a factor in simulation fidelity than the refinement domain extent, at least for the western US. This corroborates assumptions made by previous VRGCM studies that refinement domain size need only extend out as far as Hawaii when evaluating the western US and instead finer refinement should be applied over areas of complex terrain. Practically, this finding enables a core-hour saving of ~30% when running VR-CESM with the small refined domain versus the large refined domain using 48 nodes on the NERSC Cori-Haswell supercomputer.

These findings are likely generalizable to other VRGCMs that have comparable numerical order accuracy in grid-transition regions and physics parameterizations. For example, CAM-SE has third-order numerical accuracy in grid-transition regions, therefore other VRGCMs that have lower order accuracy may require a larger grid-transition region for comparable results. However, these findings are likely not generalizable to RCMs. This is because VRGCMs allow for two-way feedbacks between coarser and finer domains, whereas RCMs only enable a one-way feedback with varying degrees of influence based on domain size configuration. More specifically, using a similar experimental design to this one, western US hydroclimate simulations in RCMs may be more influenced by a westward expansion of the refinement domain over the North Pacific due to a more pronounced decoupling of larger scales (GCM boundary conditions) from regional scales (RCM simulation). Further, if boundary conditions are provided by a reanalysis dataset the relative quality of the RCM simulation would likely be impacted by the number of available observations that are assimilated in the generation of the reanalysis dataset, particularly over the Pacific Ocean.

As mentioned previously, there are still several avenues of future research that could be explored with these VR-CESM domain sensitivity experiments. One such path would be a robust evaluation of the implications of refinement domain size on the atmospheric response to teleconnections at sub-seasonal timescales (e.g., the MJO and EACS events). Given the minimal influence that refinement domain size had on North Pacific AR characteristics, particularly between the large and small refined domain, another path could be an exploration of how a warmer world may influence AR characteristics (using any of the VR-CESM grids from this study).

Acknowledgments

This research was supported by the Director, Office of Science, Office of Biological and Environmental Research of the U.S. Department of Energy Regional and Global Climate Modeling Program (RGCM) "An Integrated Evaluation of the Simulated Hydroclimate System of the Continental US" project (award no. DE-SC0016605) and "the Calibrated and Systematic Characterization, Attribution and Detection of Extremes (CASCADE)" Science Focus Area (award no. DE-AC02-05CH11231). We also acknowledge the computing resources made available by the National Energy Research Scientific Computing Center (NERSC), specifically Cori-Haswell and Cori-KNL supercomputing facilities, which were used to produce the CESM simulations. Further, we acknowledge the work of the scientists and organizations who were instrumental in generating the ERA5, PRISM and L15 reanalysis products utilized in this study to evaluate CESM model performance. The aforementioned reanalysis datasets used in this study are publicly available at their source repositories. The CESM simulations generated for this study are made available at the following NERSC Science Gateway - `https://portal.nersc.gov/archive/home/a/arhoades/Shared/www/Hyperion/`. Please notify arhoades@lbl.gov if you access and use any of the CESM datasets.

References

Alexander, M. A., I. Bladé, M. Newman, J. R. Lanzante, N. C. Lau, J. D. Scott, I. Bladé, M. Newman, J. R. Lanzante, N. C. Lau, and J. D. Scott (2002), The atmospheric bridge: The influence of ENSO teleconnections on air-sea interaction over the global oceans, *Journal of Climate*, *15*(16), 2205–2231, doi:10.1175/1520-0442(2002)015<2205:TABTIO>2.0.CO;2.

Arakawa, A., and J.-H. Jung (2011), Multiscale modeling of the moist-convective atmosphere – A review, *Atmospheric Research*, *102*(3), 263 – 285, doi:https://doi.org/10.1016/j.atmosres.2011.08.009.

Bacmeister, J. T., M. F. Wehner, R. B. Neale, A. Gettelman, C. Hannay, P. H. Lauritzen, J. M. Caron, and J. E. Truesdale (2014), Exploratory High-Resolution Climate Simulations using the Community Atmosphere Model (CAM), *Journal of Climate*, *27*(9), 3073–3099, doi:10.1175/JCLI-D-13-00387.1.

Benedict, J. J., B. Medeiros, A. C. Clement, and A. G. Pendergrass (2017), Sensitivities of the hydrologic cycle to model physics, grid resolution, and ocean type in the aquaplanet Community Atmosphere Model, *Journal of Advances in Modeling Earth Systems*, *9*(2), 1307–1324, doi:10.1002/2016MS000891.

Benedict, J. J., A. C. Clement, and B. Medeiros (2019), Atmospheric Blocking and Other Large-Scale Precursor Patterns of Landfalling Atmospheric Rivers in the North Pacific: A CESM2 Study, *Journal of Geophysical Research: Atmospheres*, *124*(21), 11,330–11,353, doi:10.1029/2019JD030790.

Benjamini, Y., and Y. Hochberg (1995), Controlling the False Discovery Rate: A Practical and Powerful Approach to Multiple Testing, *Journal of the Royal Statistical Society. Series B (Methodological)*, *57*(1), 289–300, doi:http://www.jstor.org/stable/2346101.

Bjerknes, J. (1969), Atmospheric Teleconnections from the Equatorial Pacific, *Monthly Weather Review*, *97*(3), 163–172, doi:10.1175/1520-0493(1969)097<0163:ATFTEP>2.3.CO;2.

Brisson, E., M. Demuzere, and N. P. M. van Lipzig (2016), Modelling strategies for performing convection-permitting climate simulations, *Meteorologische Zeitschrift*, *25*(2), 149–163, doi:10.1127/metz/2015/0598.

Burakowski, E. A., A. Tawfik, A. Ouimette, L. Lepine, C. Zarzycki, K. Novick, S. Ollinger, and G. Bonan (2019), Simulating surface energy fluxes using the variable-resolution Community Earth System Model (VR-CESM), *Theoretical and Applied Cli-*

matology, *138*(1-2), 115–133, doi:10.1007/s00704-019-02785-0.

Caron, L.-P., and C. G. Jones (2012), Understanding and simulating the link between african easterly waves and atlantic tropical cyclones using a regional climate model: the role of domain size and lateral boundary conditions, *Climate Dynamics*, *39*(1), 113–135, doi:10.1007/s00382-011-1160-8.

Caron, L.-P., C. G. Jones, and K. Winger (2011), Impact of resolution and downscaling technique in simulating recent atlantic tropical cylone activity, *Climate Dynamics*, *37*(5), 869–892, doi:10.1007/s00382-010-0846-7.

Cayan, D. R., K. T. Redmond, and L. G. Riddle (1999), ENSO and Hydrologic Extremes in the Western United States, *Journal of Climate*, *12*(9), 2881–2893, doi: 10.1175/1520-0442(1999)012<2881:EAHEIT>2.0.CO;2.

Chen, D., and A. Dai (2018), Dependence of estimated precipitation frequency and intensity on data resolution, *Climate dynamics*, *50*(9-10), 3625–3647, doi:https://doi.org/10.1007/s00382-017-3830-7.

Chen, D., and A. Dai (2019), Precipitation Characteristics in the Community Atmosphere Model and Their Dependence on Model Physics and Resolution, *Journal of Advances in Modeling Earth Systems*, *11*(7), 2352–2374, doi:10.1029/2018MS001536.

Christensen, J. H., and O. B. Christensen (2007), A summary of the PRUDENCE model projections of changes in European climate by the end of this century, *Climatic Change*, *81*(1), 7–30, doi:10.1007/s10584-006-9210-7.

Collins, W. D., C. M. Bitz, M. L. Blackmon, G. B. Bonan, C. S. Bretherton, J. A. Carton, P. Chang, S. C. Doney, J. J. Hack, T. B. Henderson, J. T. Kiehl, W. G. Large, D. S. McKenna, B. D. Santer, and R. D. Smith (2006), The Community Climate System Model Version 3 (CCSM3), *Journal of Climate*, *19*(11), 2122–2143, doi: 10.1175/JCLI3761.1.

Colombo, R., R. Garzonio, B. Di Mauro, M. Dumont, F. Tuzet, S. Cogliati, G. Pozzi, A. Maltese, and E. Cremonese (2019), Introducing Thermal Inertia for Monitoring Snowmelt Processes With Remote Sensing, *Geophysical Research Letters*, *46*(8), 4308–4319, doi:10.1029/2019GL082193.

Contosta, A. R., N. J. Casson, S. Garlick, S. J. Nelson, M. P. Ayres, E. A. Burakowski, J. Campbell, I. Creed, C. Eimers, C. Evans, I. Fernandez, C. Fuss, T. Huntington, K. Patel, R. Sanders-DeMott, K. Son, P. Templer, and C. Thornbrugh (2019), Northern forest winters have lost cold, snowy conditions that are important for ecosystems and human communities, *Ecological Applications*, *29*(7), e01,974, doi:10.1002/eap.1974.

Copernicus Climate Change Service (C3S) (2017), ERA5: Fifth generation of ECMWF atmospheric reanalyses of the global climate, *Copernicus Climate Change Service Climate Data Store (CDS)*, *date of access, 2019*, doi:https://cds.climate.copernicus.eu/cdsapp#!/home.

Corringham, T. W., and D. R. Cayan (2019), The Effect of El Niño on Flood Damages in the Western United States, *Weather, Climate, and Society*, *11*(3), 489–504, doi:10.1175/WCAS-D-18-0071.1.

Côté, J., S. Gravel, A. Méthot, A. Patoine, M. Roch, and A. Staniforth (1998), The Operational CMC–MRB Global Environmental Multiscale (GEM) Model. Part I: Design Considerations and Formulation, *Monthly Weather Review*, *126*(6), 1373–1395, doi:10.1175/1520-0493(1998)126<1373:TOCMGE>2.0.CO;2.

Dacre, H. F., O. Martínez-Alvarado, and C. O. Mbengue (2019), Linking Atmospheric Rivers and Warm Conveyor Belt Airflows, *Journal of Hydrometeorology*, *20*(6), 1183–1196, doi:10.1175/JHM-D-18-0175.1.

Daly, C., M. Halbleib, J. I. Smith, W. P. Gibson, M. K. Doggett, G. H. Taylor, J. Curtis, and P. P. Pasteris (2008), Physiographically sensitive mapping of climatological temperature and precipitation across the conterminous United States, *International Journal of Climatology*, *28*(15), 2031–2064, doi:10.1002/joc.1688.

Dennis, J. M., J. Edwards, K. J. Evans, O. Guba, P. H. Lauritzen, A. A. Mirin, A. St-Cyr, M. A. Taylor, and P. H. Worley (2012), CAM-SE: A scalable spectral element dynamical core for the Community Atmosphere Model, *The International Journal of High Performance Computing Applications*, *26*(1), 74–89, doi:10.1177/1094342011428142.

der Linden, P., and J. F. B. Mitchell (2009), ENSEMBLES: Climate change and its impacts-Summary of research and results from the ENSEMBLES project, *Met Office Hadley Centre, FitzRoy Road, Exeter EX1 3PB, UK*, p. 160pp, doi:http://ensembles-eu.metoffice.com/docs/Ensembles_final_report_Nov09.pdf.

Deser, C., R. Knutti, S. Solomon, and A. S. Phillips (2012), Communication of the role of natural variability in future North American climate, *Nature Climate Change*, *2*, 775–779(2012), doi:https://doi.org/10.1038/nclimate1562.

Deser, C., L. Terray, A. S. Phillips, G. D. Division, and G. D. Division (2016), Forced and internal components of winter air temperature trends over North America during the past 50 years: Mechanisms and implications, *Journal of Climate*, *29*(6), 2237–2258, doi:10.1175/JCLI-D-15-0304.1.

Deser, C., F. Lehner, K. Rodgers, T. Ault, T. Delworth, P. DiNezio, A. Fiore, C. Frankignoul, J. Fyfe, D. Horton, J. Kay, R. Knutti, N. Lovenduski, J. Marotzke, K. McKinnon, S. Minobe, J. Randerson, J. Screen, I. Simpson, and M. Ting (in press 2019), Insights from Earth system model initial-condition large ensembles and future prospects, *Nature Climate Change*, doi:10.1038/s41558-020-0731-2.

Dettinger, M. (2011), Climate Change, Atmospheric Rivers, and Floods in California - A Multimodel Analysis of Storm Frequency and Magnitude Changes, *JAWRA Journal of the American Water Resources Association*, *47*(3), 514–523, doi:10.1111/j.1752-1688.2011.00546.x.

Di Luca, A., R. de Elía, and R. Laprise (2015), Challenges in the Quest for Added Value of Regional Climate Dynamical Downscaling, *Current Climate Change Reports*, *1*(1), 10–21, doi:10.1007/s40641-015-0003-9.

Di Luca, A., D. Argüeso, J. P. Evans, R. de Elía, and R. Laprise (2016), Quantifying the overall added value of dynamical downscaling and the contribution from different spatial scales, *Journal of Geophysical Research: Atmospheres*, *121*(4), 1575–1590, doi:10.1002/2015JD024009.

Diaconescu, E. P., and R. Laprise (2013), Can added value be expected in RCM-simulated large scales?, *Climate Dynamics*, *41*(7), 1769–1800, doi:10.1007/s00382-012-1649-9.

Evans, J. P., F. Ji, C. Lee, P. Smith, D. Argüeso, and L. Fita (2014), Design of a regional climate modelling projection ensemble experiment; NARCliM, *Geoscientific Model Development*, *7*(2), 621–629, doi:10.5194/gmd-7-621-2014.

Feldl, N., and G. H. Roe (2011), Climate Variability and the Shape of Daily Precipitation: A Case Study of ENSO and the American West, *Journal of Climate*, *24*(10), 2483–2499, doi:10.1175/2010JCLI3555.1.

Folland, C., D. Stone, C. Frederiksen, D. Karoly, and J. Kinter (2014), The International CLIVAR Climate of the 20th Century Plus (C20C+) Project: Report of the Sixth Workshop, *CLIVAR Exchanges*, *19*(65), 57–59, doi:10.1016/j.ocemod.2013.10.005.Griffies.

Fox-Rabinovitz, M., J. Côté, B. Dugas, M. Déqué, and J. L. McGregor (2006), Variable resolution general circulation models: Stretched-grid model intercomparison project (SGMIP), *Journal of Geophysical Research: Atmospheres*, *111*(D16), doi:10.1029/2005JD006520.

Fox-Rabinovitz, M. S., L. L. Takacs, R. C. Govindaraju, and M. J. Suarez (2001), A Variable-Resolution Stretched-Grid General Circulation Model: Regional Climate Simulation, *Monthly Weather Review*, *129*(3), 453–469, doi:10.1175/1520-0493(2001)129<0453:AVRSGG>2.0.CO;2.

Gates, W. L., J. S. Boyle, C. Covey, C. G. Dease, C. M. Doutriaux, R. S. Drach, M. Fiorino, P. J. Gleckler, J. J. Hnilo, S. M. Marlais, T. J. Phillips, G. L. Potter, B. D. Santer, K. R. Sperber, K. E. Taylor, and D. N. Williams (1999), An Overview of the Results of the Atmospheric Model Intercomparison Project (AMIP I), *Bulletin of the American Meteorological Society*, *80*(1), 29–56, doi:10.1175/1520-0477(1999)080<0029:AOOTRO>2.0.CO;2.

Gent, P. R., G. Danabasoglu, L. J. Donner, M. M. Holland, E. C. Hunke, S. R. Jayne, D. M. Lawrence, R. B. Neale, P. J. Rasch, M. Vertenstein, P. H. Worley, Z.-L. Yang, and M. Zhang (2011), The Community Climate System Model Version 4, *Journal of Climate*, *24*(19), 4973–4991, doi:10.1175/2011JCLI4083.1.

Gettelman, A., and H. Morrison (2015), Advanced Two-Moment Bulk Microphysics for Global Models. Part I: Off-Line Tests and Comparison with Other Schemes, *Journal of Climate*, *28*(3), 1268–1287, doi:10.1175/JCLI-D-14-00102.1.

Gettelman, A., H. Morrison, S. Santos, P. Bogenschutz, and P. M. Caldwell (2015), Advanced Two–Moment Bulk Microphysics for Global Models. Part II: Global Model Solutions and Aerosol–Cloud Interactions, *Journal of Climate*, *28*(3), 1288–1307, doi:10.1175/JCLI-D-14-00103.1.

Gettelman, A., P. Callaghan, V. E. Larson, C. M. Zarzycki, J. T. Bacmeister, P. H. Lauritzen, P. A. Bogenschutz, and R. B. Neale (2018), Regional Climate Simulations With the Community Earth System Model, *Journal of Advances in Modeling Earth Systems*, *10*(6), 1245–1265, doi:10.1002/2017MS001227.

Ghan, S. J., X. Liu, R. C. Easter, R. Zaveri, P. J. Rasch, J.-H. Yoon, and B. Eaton (2012), Toward a minimal representation of aerosols in climate models: Comparative decomposition of aerosol direct, semidirect, and indirect radiative forcing, *Journal of Climate*, *25*(19), 6461–6476, doi:10.1175/JCLI-D-11-00650.1.

Gimeno, L., R. Nieto, M. Vázquez, and D. Lavers (2014), Atmospheric rivers: a mini-review, *Frontiers in Earth Science*, *2*, 2, doi:10.3389/feart.2014.00002.

Giorgi, F. (2019), Thirty Years of Regional Climate Modeling: Where Are We and Where Are We Going Next?, *Journal of Geophysical Research: Atmospheres*, *124*(11), 5696–

5723, doi:10.1029/2018JD030094.

Giorgi, F., C. Jones, G. R. Asrar, and Others (2009), Addressing climate information needs at the regional level: the CORDEX framework, *World Meteorological Organization (WMO) Bulletin*, *58*(3), 175, doi:http://wcrp.ipsl.jussieu.fr/cordex/documents/CORDEX_giorgi_WMO.pdf.

Goldenson, N., L. R. Leung, C. M. Bitz, and E. Blanchard-Wrigglesworth (2018), Influence of atmospheric rivers on mountain snowpack in the western united states, *Journal of Climate*, *31*(24), 9921–9940, doi:10.1175/JCLI-D-18-0268.1.

Guan, B., D. E. Waliser, N. P. Molotch, E. J. Fetzer, and P. J. Neiman (2012), Does the Madden–Julian Oscillation Influence Wintertime Atmospheric Rivers and Snowpack in the Sierra Nevada?, *Monthly Weather Review*, *140*(2), 325–342, doi:10.1175/MWR-D-11-00087.1.

Guan, B., N. P. Molotch, D. E. Waliser, E. J. Fetzer, and P. J. Neiman (2013), The 2010/2011 snow season in California's Sierra Nevada: Role of atmospheric rivers and modes of large-scale variability, *Water Resources Research*, *49*(10), 6731–6743, doi:10.1002/wrcr.20537.

Guan, B., D. E. Waliser, F. M. Ralph, E. J. Fetzer, and P. J. Neiman (2016), Hydrometeorological characteristics of rain-on-snow events associated with atmospheric rivers, *Geophysical Research Letters*, *43*(6), 2964–2973, doi:10.1002/2016GL067978.

Guba, O., M. A. Taylor, P. A. Ullrich, J. R. Overfelt, and M. N. Levy (2014), The spectral element method (SEM) on variable-resolution grids: evaluating grid sensitivity and resolution-aware numerical viscosity, *Geoscientific Model Development*, *7*(6), 2803–2816, doi:10.5194/gmd-7-2803-2014.

Haarsma, R. J., M. J. Roberts, P. L. Vidale, C. A. Senior, A. Bellucci, Q. Bao, P. Chang, S. Corti, N. S. Fučkar, V. Guemas, J. von Hardenberg, W. Hazeleger, C. Kodama, T. Koenigk, L. R. Leung, J. Lu, J.-J. Luo, J. Mao, M. S. Mizielinski, R. Mizuta, P. Nobre, M. Satoh, E. Scoccimarro, T. Semmler, J. Small, and J.-S. von Storch (2016), High Resolution Model Intercomparison Project (HighResMIP˜v1.0) for CMIP6, *Geoscientific Model Development*, *9*(11), 4185–4208, doi:10.5194/gmd-9-4185-2016.

Hagos, S., L. R. Leung, Q. Yang, C. Zhao, and J. Lu (2015), Resolution and Dynamical Core Dependence of Atmospheric River Frequency in Global Model Simulations, *Journal of Climate*, *28*(7), 2764–2776, doi:10.1175/JCLI-D-14-00567.1.

Hagos, S. M., L. R. Leung, J.-H. Yoon, J. Lu, and Y. Gao (2016), A projection of changes in landfalling atmospheric river frequency and extreme precipitation over western North America from the Large Ensemble CESM simulations, *Geophysical Research Letters*, *43*(3), 1357–1363, doi:10.1002/2015GL067392.

Harris, L. M., and S.-J. Lin (2013), A Two-Way Nested Global-Regional Dynamical Core on the Cubed-Sphere Grid, *Monthly Weather Review*, *141*(1), 283–306, doi:10.1175/MWR-D-11-00201.1.

Harris, L. M., S.-J. Lin, and C. Tu (2016), High-Resolution Climate Simulations Using GFDL HiRAM with a Stretched Global Grid, *Journal of Climate*, *29*(11), 4293–4314, doi:10.1175/JCLI-D-15-0389.1.

Harrison, D. E., and N. K. Larkin (1998), Seasonal U.S. temperature and precipitation anomalies associated with El Niño: Historical results and comparison with 1997-98, *Geophysical Research Letters*, *25*(21), 3959–3962, doi:10.1029/1998GL900061.

Henn, B., M. P. Clark, D. Kavetski, A. J. Newman, M. Hughes, B. McGurk, and J. D. Lundquist (2018a), Spatiotemporal patterns of precipitation inferred from streamflow observations across the Sierra Nevada mountain range, *Journal of Hydrology*, *556*, 993–1012, doi:https://doi.org/10.1016/j.jhydrol.2016.08.009.

Henn, B., A. J. Newman, B. Livneh, C. Daly, and J. D. Lundquist (2018b), An assessment of differences in gridded precipitation datasets in complex terrain, *Journal of Hydrology*, *556*, 1205–1219, doi:https://doi.org/10.1016/j.jhydrol.2017.03.008.

Herrington, A. R., and K. A. Reed (2017), An Explanation for the Sensitivity of the Mean State of the Community Atmosphere Model to Horizontal Resolution on Aquaplanets, *Journal of Climate*, *30*(13), 4781–4797, doi:10.1175/JCLI-D-16-0069.1.

Hoell, A., M. Hoerling, J. Eischeid, K. Wolter, R. Dole, J. Perlwitz, T. Xu, and L. Cheng (2016), Does El Niño intensity matter for California precipitation?, *Geophysical Research Letters*, *43*(2), 819–825, doi:10.1002/2015GL067102.

Hoerling, M. P., A. Kumar, and M. Zhong (1997), El Niño, La Niña, and the nonlinearity of their teleconnections, *Journal of Climate*, *10*(8), 1769–1786, doi:10.1175/1520-0442(1997)010<1769:ENOLNA>2.0.CO;2.

Hoskins, B. J., and D. J. Karoly (1981), The Steady Linear Response of a Spherical Atmosphere to Thermal and Orographic Forcing, *Journal of the Atmospheric Sciences*, *38*(6), 1179–1196, doi:10.1175/1520-0469(1981)038<1179:TSLROA>2.0.CO;2.

Huang, X., and P. A. Ullrich (2016), Irrigation impacts on California's climate with the variable-resolution CESM, *Journal of Advances in Modeling Earth Systems*, *8*(3), 1151–1163, doi:10.1002/2016MS000656.

Huang, X., and P. A. Ullrich (2017), The Changing Character of Twenty-First-Century Precipitation over the Western United States in the Variable-Resolution CESM, *Journal of Climate*, *30*(18), 7555–7575, doi:10.1175/JCLI-D-16-0673.1.

Huang, X., A. M. Rhoades, P. A. Ullrich, and C. M. Zarzycki (2016), An evaluation of the variable-resolution CESM for modeling California's climate, *Journal of Advances in Modeling Earth Systems*, *8*(1), 345–369, doi:10.1002/2015MS000559.

Hurrell, J. W., J. J. Hack, D. Shea, J. M. Caron, and J. Rosinski (2008), A New Sea Surface Temperature and Sea Ice Boundary Dataset for the Community Atmosphere Model, *Journal of Climate*, *21*(19), 5145–5153, doi:10.1175/2008JCLI2292.1.

Hurrell, J. W., M. M. Holland, P. R. Gent, S. Ghan, J. E. Kay, P. J. Kushner, J.-F. Lamarque, W. G. Large, D. Lawrence, K. Lindsay, W. H. Lipscomb, M. C. Long, N. Mahowald, D. R. Marsh, R. B. Neale, P. Rasch, S. Vavrus, M. Vertenstein, D. Bader, W. D. Collins, J. J. Hack, J. Kiehl, and S. Marshall (2013), The Community Earth System Model: A Framework for Collaborative Research, *Bulletin of the American Meteorological Society*, *94*(9), 1339–1360, doi:10.1175/BAMS-D-12-00121.1.

Iacono, M. J., J. S. Delamere, E. J. Mlawer, M. W. Shephard, S. A. Clough, and W. D. Collins (2008), Radiative forcing by long-lived greenhouse gases: Calculations with the AER radiative transfer models, *Journal of Geophysical Research: Atmospheres*, *113*(D13), doi:10.1029/2008JD009944.

Jiang, T., and Y. Deng (2011), Downstream modulation of North Pacific atmospheric river activity by East Asian cold surges, *Geophysical Research Letters*, *38*, L20,807, doi:10.1029/2011GL049462.

Jones, R. G., J. M. Murphy, and M. Noguer (1995), Simulation of climate change over Europe using a nested regional-climate model. I: Assessment of control climate, including sensitivity to location of lateral boundaries, *Quarterly Journal of the Royal Meteorological Society*, *121*(526), 1413–1449, doi:10.1002/qj.49712152610.

Kumar, A., E. Y. Lo, and A. D. Switzer (2019), Relationship between East Asian cold surges and synoptic patterns: A new coupling framework, *Climate*, *7*(2), 30, doi:https://doi.org/10.3390/cli7020030.

Lamjiri, M. A., M. D. Dettinger, F. M. Ralph, N. S. Oakley, and J. J. Rutz (2018), Hourly Analyses of the Large Storms and Atmospheric Rivers that Provide Most of California's Precipitation in Only 10 to 100 Hours per Year, *San Francisco Estuary and Watershed Science*, *16*(4), doi:https://doi.org/10.15447/sfews.2018v16iss4art1.

Laprise, R., R. de Elía, D. Caya, S. Biner, P. Lucas-Picher, E. Diaconescu, M. Leduc, A. Alexandru, L. Separovic, and Canadian Network for Regional Climate Modelling and Diagnostics (2008), Challenging some tenets of Regional Climate Modelling, *Meteorology and Atmospheric Physics*, *100*(1), 3–22, doi:10.1007/s00703-008-0292-9.

Lauritzen, P. H., R. D. Nair, A. R. Herrington, P. Callaghan, S. Goldhaber, J. M. Dennis, J. T. Bacmeister, B. E. Eaton, C. M. Zarzycki, M. A. Taylor, P. A. Ullrich, T. Dubos, A. Gettelman, R. B. Neale, B. Dobbins, K. A. Reed, C. Hannay, B. Medeiros, J. J. Benedict, and J. J. Tribbia (2018), NCAR Release of CAM-SE in CESM2.0: A Reformulation of the Spectral Element Dynamical Core in Dry-Mass Vertical Coordinates With Comprehensive Treatment of Condensates and Energy, *Journal of Advances in Modeling Earth Systems*, *10*(7), 1537–1570, doi:10.1029/2017MS001257.

Lavers, D. A., D. E. Waliser, F. M. Ralph, and M. D. Dettinger (2016), Predictability of horizontal water vapor transport relative to precipitation: Enhancing situational awareness for forecasting western U.S. extreme precipitation and flooding, *Geophysical Research Letters*, *43*(5), 2275–2282, doi:10.1002/2016GL067765.

Lawrence, D. M., R. A. Fisher, C. D. Koven, K. W. Oleson, S. C. Swenson, G. Bonan, N. Collier, B. Ghimire, L. van Kampenhout, D. Kennedy, E. Kluzek, P. J. Lawrence, F. Li, H. Li, D. Lombardozzi, W. J. Riley, W. J. Sacks, M. Shi, M. Vertenstein, W. R. Wieder, C. Xu, A. A. Ali, A. M. Badger, G. Bisht, M. A. Brunke, S. P. Burns, J. Buzan, M. Clark, A. Craig, K. Dahlin, B. Drewniak, J. B. Fisher, M. Flanner, A. M. Fox, P. Gentine, F. Hoffman, G. Keppel-Aleks, R. Knox, S. Kumar, J. Lenaerts, L. R. Leung, W. H. Lipscomb, Y. Lu, P. A., J. D. Pelletier, J. Perket, J. T. Randerson, D. M. Ricciuto, B. M. Sanderson, A. Slater, Z. M. Subin, J. Tang, R. Q. Thomas, M. V. Martin, and X. Zeng (2019), The Community Land Model version 5: Description of new features, benchmarking, and impact of forcing uncertainty, *Journal of Advances in Modeling Earth Systems*, doi:10.1029/2018MS001583.

Leduc, M., and R. Laprise (2009), Regional climate model sensitivity to domain size, *Climate Dynamics*, *32*(6), 833–854, doi:10.1007/s00382-008-0400-z.

Lee, S. K., H. Lopez, E. S. Chung, P. DiNezio, S. W. Yeh, and A. T. Wittenberg (2018), On the Fragile Relationship Between El Niño and California Rainfall, *Geophysical Research Letters*, *45*(2), 907–915, doi:10.1002/2017GL076197.

Livneh, B., T. J. Bohn, D. W. Pierce, F. Munoz-Arriola, B. Nijssen, R. Vose, D. R. Cayan, and L. Brekke (2015), A spatially comprehensive, hydrometeorological data set for Mexico, the U.S., and Southern Canada 1950–2013, *Scientific Data*, *2*(150042), doi: doi:10.1038/sdata.2015.42.

Lucas-Picher, P., R. Laprise, and K. Winger (2017), Evidence of added value in North American regional climate model hindcast simulations using ever-increasing horizontal resolutions, *Climate Dynamics*, *48*(7), 2611–2633, doi:10.1007/s00382-016-3227-z.

Margulis, S. A., G. Cortes, M. Girotto, and M. Durand (2016), A Landsat-Era Sierra Nevada Snow Reanalysis (1985–2015), *Journal of Hydrometeorology*, *17*(4), 1203–1221, doi:10.1175/JHM-D-15-0177.1.

Matte, D., R. Laprise, and J. M. Thériault (2016), Comparison between high-resolution climate simulations using single- and double-nesting approaches within the Big-Brother experimental protocol, *Climate Dynamics*, *47*(12), 3613–3626, doi:10.1007/s00382-016-3031-9.

Matte, D., R. Laprise, J. M. Thériault, and P. Lucas-Picher (2017), Spatial spin-up of fine scales in a regional climate model simulation driven by low-resolution boundary conditions, *Climate Dynamics*, *49*(1), 563–574, doi:10.1007/s00382-016-3358-2.

McGregor, J. L. (2005), Geostrophic Adjustment for Reversibly Staggered Grids, *Monthly Weather Review*, *133*(5), 1119–1128, doi:10.1175/MWR2908.1.

McPhaden, M. J., S. E. Zebiak, and M. H. Glantz (2006), ENSO as an Integrating Concept in Earth Science, *Science*, *314*(5806), 1740–1745, doi:10.1126/science.1132588.

Mearns, L. O., R. Arritt, S. Biner, M. S. Bukovsky, S. McGinnis, S. Sain, D. Caya, J. Correia, D. Flory, W. Gutowski, E. S. Takle, R. Jones, R. Leung, W. Moufouma-Okia, L. McDaniel, A. M. B. Nunes, Y. Qian, J. Roads, L. Sloan, and M. Snyder (2012), The North American Regional Climate Change Assessment Program: Overview of Phase I Results, *Bulletin of the American Meteorological Society*, *93*(9), 1337–1362, doi: 10.1175/BAMS-D-11-00223.1.

Miguez-Macho, G., G. L. Stenchikov, and A. Robock (2004), Spectral nudging to eliminate the effects of domain position and geometry in regional climate model simulations, *Journal of Geophysical Research: Atmospheres*, *109*(D13), doi:10.1029/2003JD004495.

Neale, R. B., J. H. Richter, and M. Jochum (2008), The impact of convection on ENSO: From a delayed oscillator to a series of events, *Journal of Climate*, *21*(22), 5904–5924, doi:10.1175/2008JCLI2244.1.

Neale, R. B., C.-C. Chen, A. Gettelman, P. H. Lauritzen, S. Park, D. L. Williamson, A. J. Conley, R. Garcia, D. Kinnison, J.-F. Lamarque, D. Marsh, M. Mills, A. K. Smith, S. Tilmes, F. Vitt, P. Cameron-Smith, W. D. Collins, M. J. Iacono, and R. C. Easter, X. Liu, S. J. Ghan, P. J. Rasch, and M. A. Taylor (2010), Description of the {NCAR} {C}ommunity {A}tmosphere {M}odel ({CAM} 5.0), *NCAR Technical Note NCAR/TN-486+STR*, National Center for Atmospheric Research, Boulder, Colorado, doi: http://www.cesm.ucar.edu/models/cesm1.0/cam/docs/description/cam5_desc.pdf.

Neelin, J. D., D. S. Battisti, A. C. Hirst, F.-F. Jin, Y. Wakata, T. Yamagata, and S. E. Zebiak (1998), ENSO theory, *Journal of Geophysical Research: Oceans*, *103*(C7), 14,261–14,290, doi:10.1029/97JC03424.

Neiman, P. J., F. M. Ralph, G. A. Wick, J. D. Lundquist, and M. D. Dettinger (2008), Meteorological Characteristics and Overland Precipitation Impacts of Atmospheric Rivers Affecting the West Coast of North America Based on Eight Years of SSM/I Satellite Observations, *Journal of Hydrometeorology*, *9*(1), 22–47, doi:10.1175/2007JHM855.1.

O'Brien, J. P., T. A. O'Brien, C. M. Patricola, and S.-Y. S. Y. Wang (2019), Metrics for understanding large-scale controls of multivariate temperature and precipitation variability, *Climate Dynamics*, *53*, 3805–3823, doi:10.1007/s00382-019-04749-6.

O'Brien, T. A., W. D. Collins, K. Kashinath, O. Rübel, S. Byna, J. Gu, H. Krishnan, and P. A. Ullrich (2016), Resolution dependence of precipitation statistical fidelity in hindcast simulations, *Journal of Advances in Modeling Earth Systems*, *8*(2), 976–990, doi: 10.1002/2016MS000671.

Park, S., and C. S. Bretherton (2009), The University of Washington shallow convection and moist turbulence schemes and their impact on climate simulations with the Community Atmosphere Model, *Journal of Climate*, *22*(12), 3449–3469, doi:10.1175/2008JCLI2557.1.

Park, S., C. S. Bretherton, and P. J. Rasch (2014), Integrating cloud processes in the Community Atmosphere Model, Version 5, *Journal of Climate*, *27*(18), 6821–6856, doi: 10.1175/JCLI-D-14-00087.1.

Patricola, C. M., J. P. O'Brien, M. D. Risser, A. M. Rhoades, T. A. O'Brien, P. A. Ullrich, D. A. Stone, and W. D. Collins (2019), Maximizing enso as a source of western us hydroclimate predictability, *Climate Dynamics*, pp. 1–22, doi:10.1007/s00382-019-05004-8.

Payne, A. E., and G. Magnusdottir (2014), Dynamics of Landfalling Atmospheric Rivers over the North Pacific in 30 Years of MERRA Reanalysis, *Journal of Climate*, *27*(18), 7133–7150, doi:10.1175/JCLI-D-14-00034.1.

Philander, S. G. H. (1985), El Niño and La Niña, *Journal of the Atmospheric Sciences*, *42*(23), 2652–2662, doi:10.1175/1520-0469(1985)042<2652:ENALN>2.0.CO;2.

Poan, E. D., P. Gachon, R. Laprise, R. Aider, and G. Dueymes (2018), Investigating added value of regional climate modeling in North American winter storm track simulations, *Climate Dynamics*, *50*(5), 1799–1818, doi:10.1007/s00382-017-3723-9.

Rahimi, S. R., C. Wu, X. Liu, and H. Brown (2019), Exploring a variable-resolution approach for simulating regional climate over the Tibetan Plateau using VR-CESM, *Journal of Geophysical Research: Atmospheres*, *124*, 4490–4513, doi:10.1029/2018JD028925.

Ralph, F. M., and M. D. Dettinger (2011), Storms, floods, and the science of atmospheric rivers, *Eos, Transactions American Geophysical Union*, *92*(32), 265–266, doi:10.1029/2011EO320001.

Ralph, F. M., P. J. Neiman, G. A. Wick, S. I. Gutman, M. D. Dettinger, D. R. Cayan, and A. B. White (2006), Flooding on California's Russian River: Role of atmospheric rivers, *Geophysical Research Letters*, *33*(13), doi:10.1029/2006GL026689.

Ralph, F. M., J. Intrieri, D. Andra, R. Atlas, S. Boukabara, D. Bright, P. Davidson, B. Entwistle, J. Gaynor, S. Goodman, J.-G. Jiing, A. Harless, J. Huang, G. Jedlovec, J. Kain, S. Koch, B. Kuo, J. Levit, S. Murillo, L. P. Riishojgaard, T. Schneider, R. Schneider, T. Smith, and S. Weiss (2013), The Emergence of Weather-Related Test Beds Linking Research and Forecasting Operations, *Bulletin of the American Meteorological Society*, *94*(8), 1187–1211, doi:10.1175/BAMS-D-12-00080.1.

Ralph, F. M., M. D. Dettinger, M. M. Cairns, T. J. Galarneau, and J. Eylander (2018), Defining "Atmospheric River": How the Glossary of Meteorology Helped Resolve a Debate, *Bulletin of the American Meteorological Society*, *99*(4), 837–839, doi:10.1175/BAMS-D-17-0157.1.

Ralph, F. M., J. J. Rutz, J. M. Cordeira, M. Dettinger, M. Anderson, D. Reynolds, L. J. Schick, and C. Smallcomb (2019), A Scale to Characterize the Strength and Impacts of Atmospheric Rivers, *Bulletin of the American Meteorological Society*, *100*(2), 269–289, doi:10.1175/BAMS-D-18-0023.1.

Rasmusson, E. M., and J. M. Wallace (1983), Meteorological Aspects of the El Nino/Southern Oscillation, *Science*, *222*(4629), 1195–1202, doi:10.1126/science.222.4629.1195.

Rauscher, S. A., and T. D. Ringler (2014), Impact of Variable-Resolution Meshes on Midlatitude Baroclinic Eddies Using CAM-MPAS-A, *Monthly Weather Review*, *142*(11), 4256–4268, doi:10.1175/MWR-D-13-00366.1.

Rauscher, S. A., T. D. Ringler, W. C. Skamarock, and A. A. Mirin (2013), Exploring a Global Multiresolution Modeling Approach Using Aquaplanet Simulations, *Journal of Climate*, *26*(8), 2432–2452, doi:10.1175/JCLI-D-12-00154.1.

Rauscher, S. A., T. A. O'Brien, C. Piani, E. Coppola, F. Giorgi, W. D. Collins, and P. M. Lawston (2016), A multimodel intercomparison of resolution effects on precipitation: simulations and theory, *Climate Dynamics*, *47*(7), 2205–2218, doi:10.1007/s00382-015-2959-5.

Rhoades, A. M., X. Huang, P. A. Ullrich, and C. M. Zarzycki (2016), Characterizing Sierra Nevada Snowpack Using Variable-Resolution CESM, *Journal of Applied Meteorology and Climatology*, *55*(1), 173–196, doi:10.1175/JAMC-D-15-0156.1.

Rhoades, A. M., P. A. Ullrich, and C. M. Zarzycki (2018a), Projecting 21st century snowpack trends in western USA mountains using variable-resolution CESM, *Climate Dynamics*, *50*(1), 261–288, doi:10.1007/s00382-017-3606-0.

Rhoades, A. M., P. A. Ullrich, C. M. Zarzycki, H. Johansen, S. A. Margulis, H. Morrison, Z. Xu, and W. D. Collins (2018b), Sensitivity of Mountain Hydroclimate Simulations in Variable-Resolution CESM to Microphysics and Horizontal Resolution, *Journal of Advances in Modeling Earth Systems*, *10*(6), 1357–1380, doi:10.1029/2018MS001326.

Rhoades, A. M., A. D. Jones, and P. A. Ullrich (2018c), Assessing Mountains as Natural Reservoirs With a Multimetric Framework, *Earth's Future*, *6*(9), 1221–1241, doi:10.1002/2017EF000789.

Rhoades, A. M., A. D. Jones, and P. A. Ullrich (2018d), The Changing Character of the California Sierra Nevada as a Natural Reservoir, *Geophysical Research Letters*, *45*(23), 13,008–13,019, doi:10.1029/2018GL080308.

Sabin, T. P., C. A. Babu, and P. V. Joseph (2013), SST-convection relation over tropical oceans, *International Journal of Climatology*, *33*(6), 1424–1435, doi:10.1002/joc.3522.

Sakaguchi, K., L. R. Leung, C. Zhao, Q. Yang, J. Lu, S. Hagos, S. A. Rauscher, L. Dong, T. D. Ringler, and P. H. Lauritzen (2015), Exploring a Multiresolution Approach Using AMIP Simulations, *Journal of Climate*, *28*(14), 5549–5574, doi:10.1175/JCLI-D-14-00729.1.

Sakaguchi, K., J. Lu, L. R. Leung, C. Zhao, Y. Li, and S. Hagos (2016), Sources and pathways of the upscale effects on the Southern Hemisphere jet in MPAS-CAM4 variable-resolution simulations, *Journal of Advances in Modeling Earth Systems*, *8*(4), 1786–1805, doi:10.1002/2016MS000743.

Shields, C. A., and J. T. Kiehl (2016a), Simulating the Pineapple Express in the half degree Community Climate System Model, CCSM4, *Geophysical Research Letters*, *43*(14), 7767–7773, doi:10.1002/2016GL069476.

Shields, C. A., and J. T. Kiehl (2016b), Atmospheric river landfall-latitude changes in future climate simulations, *Geophysical Research Letters*, *43*(16), 8775–8782, doi:10.1002/2016GL070470.

Shields, C. A., J. J. Rutz, L.-Y. Leung, F. M. Ralph, M. Wehner, B. Kawzenuk, J. M. Lora, E. McClenny, T. Osborne, A. E. Payne, P. Ullrich, A. Gershunov, N. Goldenson, B. Guan, Y. Qian, A. M. Ramos, C. Sarangi, S. Sellars, I. Gorodetskaya, K. Kashinath, V. Kurlin, K. Mahoney, G. Muszynski, R. Pierce, A. C. Subramanian, R. Tome, D. Waliser, D. Walton, G. Wick, A. Wilson, D. Lavers, Prabhat, A. Collow, H. Krishnan, G. Magnusdottir, and P. Nguyen (2018), Atmospheric River Tracking Method Intercomparison Project (ARTMIP): project goals and experimental design, *Geoscientific Model Development*, *11*(6), 2455–2474, doi:10.5194/gmd-11-2455-2018.

Stone, D. A., N. Christidis, C. Folland, S. Perkins-kirkpatrick, J. Perlwitz, H. Shiogama, M. F. Wehner, P. Wolski, S. Cholia, H. Krishnan, D. Murray, O. Angélil, U. Beyerle, A. Ciavarella, A. Dittus, X.-w. Quan, M. Tadross, and L. Berkeley (2019), Experiment design of the International CLIVAR C20C+ Detection and Attribution project, *Weather and Climate Extremes*, *24*, 100,206, doi:10.1016/j.wace.2019.100206.

Sun, Q., C. Miao, Q. Duan, H. Ashouri, S. Sorooshian, and K.-L. Hsu (2018), A Review of Global Precipitation Data Sets: Data Sources, Estimation, and Intercomparisons, *Reviews of Geophysics*, *56*(1), 79–107, doi:10.1002/2017RG000574.

The NCAR Command Language (Version 6.6.2) (2019), Boulder, Colorado: UCAR/NCAR/CISL/TDD, http://dx.doi.org/10.5065/D6WD3XH5.

Timmermann, A., S.-I. An, J.-S. Kug, F.-F. Jin, W. Cai, A. Capotondi, K. Cobb, M. Lengaigne, M. J. McPhaden, M. F. Stuecker, K. Stein, A. T. Wittenberg, K.-S. Yun, T. Bayr, H.-C. Chen, Y. Chikamoto, B. Dewitte, D. Dommenget, P. Grothe, E. Guilyardi, Y.-G. Ham, M. Hayashi, S. Ineson, D. Kang, S. Kim, W. Kim, J.-Y. Lee, T. Li, J.-J. Luo, S. McGregor, Y. Planton, S. Power, H. Rashid, H.-L. Ren, A. Santoso, K. Takahashi, A. Todd, G. G. Wang, R. Xie, W.-H. Yang, S.-W. Yeh, J. Yoon, E. Zeller, and X. Zhang (2018), El Niño–Southern Oscillation complexity, *Nature*, *559*(7715), 535–545, doi:10.1038/s41586-018-0252-6.

Timmermans, B., M. Wehner, D. Cooley, T. O'Brien, and H. Krishnan (2019), An evaluation of the consistency of extremes in gridded precipitation data sets, *Climate Dynamics*, *52*, 6651–6670, doi:10.1007/s00382-018-4537-0.

Trenberth, K. E., G. W. Branstator, D. Karoly, A. Kumar, N.-C. Lau, and C. Ropelewski (1998), Progress during TOGA in understanding and modeling global teleconnections associated with tropical sea surface temperatures, *Journal of Geophysical Research: Oceans*, *103*(C7), 14,291–14,324, doi:10.1029/97JC01444.

Ullrich, P. A. (2014), SQuadGen: Spherical Quadrilateral Grid Generator, available online at http://climate.ucdavis.edu/squadgen.php.

Ullrich, P. A., and M. A. Taylor (2015), Arbitrary-Order Conservative and Consistent Remapping and a Theory of Linear Maps: Part I, *Monthly Weather Review*, *143*(6), 2419–2440, doi:10.1175/MWR-D-14-00343.1.

Ullrich, P. A., and C. M. Zarzycki (2017), TempestExtremes: a framework for scale-insensitive pointwise feature tracking on unstructured grids, *Geoscientific Model Development*, *10*(3), 1069–1090, doi:10.5194/gmd-10-1069-2017.

Ullrich, P. A., D. Devendran, and H. Johansen (2016), Arbitrary-Order Conservative and Consistent Remapping and a Theory of Linear Maps: Part II, *Monthly Weather Review*, *144*(4), 1529–1549, doi:10.1175/MWR-D-15-0301.1.

Ullrich, P. A., C. Jablonowski, J. Kent, P. H. Lauritzen, R. Nair, K. A. Reed, C. M. Zarzycki, D. M. Hall, D. Dazlich, R. Heikes, C. Konor, D. Randall, T. Dubos, Y. Meurdesoif, X. Chen, L. Harris, C. Kühnlein, V. Lee, A. Qaddouri, C. Girard, M. Giorgetta, D. Reinert, J. Klemp, S.-H. Park, W. Skamarock, H. Miura, T. Ohno, R. Yoshida, R. Walko, A. Reinecke, and K. Viner (2017), DCMIP2016: a review of non-hydrostatic dynamical core design and intercomparison of participating models, *Geoscientific Model Development*, *10*(12), 4477–4509, doi:10.5194/gmd-10-4477-2017.

Ullrich, P. A., Z. Xu, A. M. Rhoades, M. D. Dettinger, J. F. Mount, A. D. Jones, and P. Vahmani (2018), California's Drought of the Future: A Midcentury Recreation of the Exceptional Conditions of 2012-2017, *Earth's Future*, *6*, 1568–1587, doi:10.1029/2018EF001007.

van Kampenhout, L., J. T. M. Lenaerts, W. H. Lipscomb, W. J. Sacks, D. M. Lawrence, A. G. Slater, and M. R. van den Broeke (2017), Improving the Representation of Polar Snow and Firn in the Community Earth System Model, *Journal of Advances in Modeling Earth Systems*, *9*(7), 2583–2600, doi:10.1002/2017MS000988.

van Kampenhout, L., A. M. Rhoades, A. R. Herrington, C. M. Zarzycki, J. T. M. Lenaerts, W. J. Sacks, and M. R. van den Broeke (2019), Regional Grid Refinement in an Earth System Model: Impacts on the Simulated Greenland Surface Mass Balance, *The Cryosphere*, *13*, 1547–1564, doi:https://doi.org/10.5194/tc-13-1547-2019.

Vano, J. A., K. Miller, M. D. Dettinger, R. Cifelli, D. Curtis, A. Dufour, J. R. Olsen, and A. M. Wilson (2019), Hydroclimatic Extremes as Challenges for the Water Management Community: Lessons from Oroville Dam and Hurricane Harvey, *Bulletin of the American Meteorological Society*, *100*(1), S9–S14, doi:10.1175/BAMS-D-18-0219.1.

Waliser, D. E., M. W. Moncrieff, D. Burridge, A. H. Fink, D. Gochis, B. N. Goswami, B. Guan, P. Harr, J. Heming, H.-H. Hsu, C. Jakob, M. Janiga, R. Johnson, S. Jones, P. Knippertz, J. Marengo, H. Nguyen, M. Pope, Y. Serra, C. Thorncroft, M. Wheeler, R. Wood, and S. Yuter (2012), The "Year" of Tropical Convection (May 2008âĂŞApril 2010): Climate Variability and Weather Highlights, *Bulletin of the American Meteorological Society*, *93*(8), 1189–1218, doi:10.1175/2011BAMS3095.1.

Walton, D., and A. Hall (2018), An Assessment of High-Resolution Gridded Temperature Datasets over California, *Journal of Climate*, *31*(10), 3789–3810, doi:10.1175/JCLI-D-17-0410.1.

Wang, M., and P. Ullrich (2018), Marine Air Penetration in California's Central Valley: Meteorological Drivers and the Impact of Climate Change, *Journal of Applied Meteorology and Climatology*, *57*(1), 137–154, doi:10.1175/JAMC-D-17-0089.1.

Wang, M., P. Ullrich, and D. Millstein (2018), The future of wind energy in California: Future projections with the Variable-Resolution CESM, *Renewable Energy*, *127*, 242–257, doi:https://doi.org/10.1016/j.renene.2018.04.031.

Wehner, M. F., K. A. Reed, F. Li, Prabhat, J. Bacmeister, C.-T. Chen, C. Paciorek, P. J. Gleckler, K. R. Sperber, W. D. Collins, A. Gettelman, and C. Jablonowski (2014), The effect of horizontal resolution on simulation quality in the Community Atmospheric Model, CAM5.1, *Journal of Advances in Modeling Earth Systems*, *6*(4), 980–997, doi: 10.1002/2013MS000276.

White, A. B., B. J. Moore, D. J. Gottas, and P. J. Neiman (2019), Winter Storm Conditions Leading to Excessive Runoff above California's Oroville Dam during January and February 2017, *Bulletin of the American Meteorological Society*, *100*(1), 55–70, doi: 10.1175/BAMS-D-18-0091.1.

Wilks, D. S. (2016), "The Stippling Shows Statistically Significant Grid Points": How Research Results are Routinely Overstated and Overinterpreted, and What to Do about It, *Bulletin of the American Meteorological Society*, *97*(12), 2263–2273, doi: 10.1175/BAMS-D-15-00267.1.

Williams, I. N., and C. M. Patricola (2018), Diversity of ENSO Events Unified by Convective Threshold Sea Surface Temperature: A Nonlinear ENSO Index, *Geophysical Research Letters*, *45*(17), 9236–9244, doi:10.1029/2018GL079203.

Williamson, D. L. (2008), Convergence of aqua-planet simulations with increasing resolution in the Community Atmospheric Model, Version 3, *Tellus*, *60A*, 848–862, doi: doi:10.1111/j.1600-0870.2008.00339.x.

Wu, C., X. Liu, Z. Lin, A. M. Rhoades, P. A. Ullrich, C. M. Zarzycki, Z. Lu, and S. R. Rahimi-Esfarjani (2017), Exploring a Variable-Resolution Approach for Simulating Regional Climate in the Rocky Mountain Region Using the VR-CESM, *Journal of Geophysical Research: Atmospheres*, *122*(20), 10,939–10,965, doi:10.1002/2017JD027008.

Wu, C., X. Liu, Z. Lin, S. R. Rahimi-Esfarjani, and Z. Lu (2018), Impacts of absorbing aerosol deposition on snowpack and hydrologic cycle in the Rocky Mountain region based on variable-resolution CESM (VR-CESM) simulations, *Atmospheric Chemistry and Physics*, *18*(2), 511–533, doi:10.5194/acp-18-511-2018.

Xu, Y., A. Jones, and A. Rhoades (2019), A quantitative method to decompose SWE differences between regional climate models and reanalysis datasets, *Scientific Reports*, *9*, 16,520, doi:10.1038/s41598-019-52880-5.

Xu, Z., A. M. Rhoades, H. Johansen, P. A. Ullrich, and W. D. Collins (2018), An Intercomparison of GCM and RCM Dynamical Downscaling for Characterizing the Hydroclimatology of California and Nevada, *Journal of Hydrometeorology*, *19*(9), 1485–1506, doi:10.1175/JHM-D-17-0181.1.

Xue, Y., Z. Janjic, J. Dudhia, R. Vasic, and F. D. Sales (2014), A review on regional dynamical downscaling in intraseasonal to seasonal simulation/prediction and major factors that affect downscaling ability, *Atmospheric Research*, *147-148*, 68–85, doi: https://doi.org/10.1016/j.atmosres.2014.05.001.

Yessad, K., and P. Bénard (1996), Introduction of a local mapping factor in the spectral part of the Météo-France global variable mesh numerical forecast model, *Quarterly Journal of the Royal Meteorological Society*, *122*(535), 1701–1719, doi:10.1002/qj.49712253511.

Zarzycki, C. M. (2016), Tropical Cyclone Intensity Errors Associated with Lack of Two-Way Ocean Coupling in High-Resolution Global Simulations, *Journal of Climate*, *29*(23), 8589–8610, doi:10.1175/JCLI-D-16-0273.1.

Zarzycki, C. M., and C. Jablonowski (2014), A multidecadal simulation of Atlantic tropical cyclones using a variable-resolution global atmospheric general circulation model, *Journal of Advances in Modeling Earth Systems*, *6*(3), 805–828, doi:10.1002/2014MS000352.

Zarzycki, C. M., and P. A. Ullrich (2017), Assessing sensitivities in algorithmic detection of tropical cyclones in climate data, *Geophysical Research Letters*, *44*(2), 1141–1149, doi:10.1002/2016GL071606.

Zarzycki, C. M., C. Jablonowski, and M. A. Taylor (2014a), Using Variable-Resolution Meshes to Model Tropical Cyclones in the Community Atmosphere Model, *Monthly Weather Review*, *142*(3), 1221–1239, doi:10.1175/MWR-D-13-00179.1.

Zarzycki, C. M., M. N. Levy, C. Jablonowski, J. R. Overfelt, M. A. Taylor, and P. A. Ullrich (2014b), Aquaplanet Experiments Using CAM's Variable-Resolution Dynamical Core, *Journal of Climate*, *27*(14), 5481–5503, doi:10.1175/JCLI-D-14-00004.1.

Zarzycki, C. M., C. Jablonowski, D. R. Thatcher, and M. A. Taylor (2015), Effects of Localized Grid Refinement on the General Circulation and Climatology in the Community Atmosphere Model, *Journal of Climate*, *28*(7), 2777–2803, doi:10.1175/JCLI-D-14-00599.1.

Zarzycki, C. M., K. A. Reed, J. T. Bacmeister, A. P. Craig, S. C. Bates, and N. A. Rosenbloom (2016), Impact of surface coupling grids on tropical cyclone extremes in high-resolution atmospheric simulations, *Geoscientific Model Development*, *9*(2), 779–788, doi:10.5194/gmd-9-779-2016.

Zhou, Y., H. Kim, and B. Guan (2018), Life Cycle of Atmospheric Rivers: Identification and Climatological Characteristics, *Journal of Geophysical Research: Atmospheres*, *123*(22), 12,712–715,725, doi:10.1029/2018JD029180.

Zhu, Y., and R. E. Newell (1998), A Proposed Algorithm for Moisture Fluxes from Atmospheric Rivers, *Monthly Weather Review*, *126*(3), 725–735, doi:10.1175/1520-0493(1998)126<0725:APAFMF>2.0.CO;2.